Advection-Dominated Accretion around Black Holes†

By R A M E S H   N A R A Y A N
R O H A N   M A H A D E V A N
AND
E L I O T   Q U A T A E R T

Harvard–Smithsonian Center for Astrophysics, 60 Garden Street, Cambridge, MA 02138, USA

This article reviews the physics of advection-dominated accretion flows (ADAFs) and describes applications to several black hole X-ray binaries and galactic nuclei. The possibility of using ADAFs to explore the event horizons of black holes is highlighted.

1. Introduction

Accretion processes around black holes almost inevitably involve rotating gas flows. Consequently, there is great interest in self–consistent solutions of the hydrodynamic equations of viscous differentially–rotating flows. Four solutions are currently known (see Chen et al. 1995 for a discussion). In these solutions viscosity transports angular momentum outward, allowing the accreting gas to spiral in toward the central mass. Viscosity also acts as a source of heat; some or all of this heat is radiated, leading to the observed spectrum.

The most famous of the four solutions is the thin disk model developed by Shakura & Sunyaev (1973), Novikov & Thorne (1973), Lynden–Bell & Pringle (1974) and others (see Pringle 1981 and Frank et al. 1992 for reviews). The accreting gas forms a geometrically thin, optically thick disk, and produces a quasi–blackbody spectrum. The effective temperature of the radiation is in the range $10^5 - 10^7$ K, depending on the black hole mass and the accretion rate ($T_{\text{eff}} \propto M^{-1/4}\dot{M}^{1/4}$). The thin disk solution has been used to model a large number of astrophysical systems.

Shapiro, Lightman and Eardley (1976; hereafter SLE; see also Björnsson & Svensson 1991 and Luo & Liang 1994) discovered a second, much hotter self–consistent solution in which the accreting gas forms a two temperature plasma with the ion temperature greater than the electron temperature ($T_i \sim 10^{11}$K, $T_e \sim 10^8-10^9$K). The gas is optically thin and produces a power–law spectrum at X–ray and soft γ–ray energies. The SLE solution is, however, thermally unstable (Piran 1978), and is therefore not considered viable for real flows.

At super–Eddington accretion rates, a third solution is present (Katz 1977; Begelman 1978; Abramowicz et al. 1988; see also Begelman & Meier 1982; Eggum, Coroniti, & Katz 1988), in which the large optical depth of the inflowing gas traps most of the radiation and carries it inward, or "advects" it, into the central black hole. This solution is referred to as an optically thick advection–dominated accretion flow (optically thick ADAF). A full analysis of the dynamics of the solution was presented in an important paper by Abramowicz et al. (1988).

A fourth solution is present in the opposite limit of low, sub–Eddington, accretion rates (Ichimaru 1977; Rees et al. 1982; Narayan & Yi 1994, 1995a, 1995b; Abramowicz

---

† To appear in *The Theory of Black Hole Accretion Discs*, eds. M. A. Abramowicz, G. Bjornsson, & J. E. Pringle (Cambridge University Press)

et al. 1995). In this solution, the accreting gas has a very low density and is unable to cool efficiently within an accretion time. The viscous energy is therefore stored in the gas as thermal energy instead of being radiated, and is advected onto the central star. The gas is optically thin and adopts a two–temperature configuration, as in the SLE solution. The solution is therefore referred to as an optically thin ADAF or a two–temperature ADAF.

This article reviews ADAFs around black holes, with an emphasis on two–temperature ADAFs.

2. Dynamics of ADAFs

2.1. *Basic Equations*

Consider a steady axisymmetric accretion flow. The dynamics of the flow are described by the following four height-integrated differential equations, which express the conservation of mass, radial momentum, angular momentum, and energy:

$$\frac{d}{dR}(\rho R H v) = 0, \tag{2.1}$$

$$v\frac{dv}{dR} - \Omega^2 R = -\Omega_K^2 R - \frac{1}{\rho}\frac{d}{dR}(\rho c_s^2), \tag{2.2}$$

$$v\frac{d(\Omega R^2)}{dR} = \frac{1}{\rho R H}\frac{d}{dR}\left(\nu\rho R^3 H\frac{d\Omega}{dR}\right), \tag{2.3}$$

$$\rho v T\frac{ds}{dR} = q^+ - q^- = \rho\nu R^2\left(\frac{d\Omega}{dR}\right)^2 - q^- \equiv f\nu\rho R^2\left(\frac{d\Omega}{dR}\right)^2, \tag{2.4}$$

where ρ is the density of the gas, R is the radius, $H \sim c_s/\Omega_K$ is the vertical scale height, v is the radial velocity, c_s is the isothermal sound speed, T is the temperature of the gas (mean temperature in the case of a two temperature gas), Ω is the angular velocity, Ω_K is the Keplerian angular velocity, s is the specific entropy of the gas, q^+ is the energy generated by viscosity per unit volume, and q^- is the radiative cooling per unit volume. The quantity on the left in equation (2.4) is the rate of advection of energy per unit volume. The parameter f is thus the ratio of the advected energy to the heat generated and measures the degree to which the flow is advection–dominated. The kinematic viscosity coefficient, ν, is generally parameterized via the α prescription of Shakura & Sunyaev (1973),

$$\nu \equiv \alpha c_s H = \alpha\frac{c_s^2}{\Omega_K}, \tag{2.5}$$

where α is assumed to be independent of R. The steady state mass conservation equation implies a constant accretion rate throughout the flow:

$$\dot{M} = (2\pi R)(2H)\rho|v| = \text{constant}. \tag{2.6}$$

It is useful to rewrite the energy equation (2.4) compactly as

$$q^{\text{adv}} = q^+ - q^-, \tag{2.7}$$

where q^{adv} represents the advective transport of energy (usually a form of cooling). Depending on the relative magnitudes of the terms in this equation, three regimes of accretion may be identified:

• $q^+ \simeq q^- \gg q^{\text{adv}}$. This corresponds to a cooling-dominated flow where all the energy

released by viscous stresses is radiated; the amount of energy advected is negligible. The thin disk solution and the SLE solution correspond to this regime.

• $q^{\text{adv}} \simeq q^+ \gg q^-$. This corresponds to an ADAF where almost all the viscous energy is stored in the gas and is deposited into the black hole. The amount of cooling is negligible compared with the heating. For a given $\dot{M}$, an ADAF is much less luminous than a cooling-dominated flow.

• $-q^{\text{adv}} \simeq q^- \gg q^+$. This corresponds to a flow where energy generation is negligible, but the entropy of the inflowing gas is converted to radiation. Examples are Bondi accretion, Kelvin–Helmholtz contraction during the formation of a star, and cooling flows in galaxy clusters.

2.2. *Self–Similar Solution*

Analytical approximations to the structure of optically thick and optically thin ADAFs have been derived by Narayan & Yi (1994). Assuming Newtonian gravity ($\Omega_K^2 = GM/R^3$) and taking f to be independent of R, they showed that equations (2.1)–(2.4) have the following self–similar solution (see also Spruit et al. 1987):

$$v(R) = -\frac{(5 + 2\epsilon')}{3\alpha^2} g(\alpha, \epsilon') \alpha v_{\text{ff}}, \tag{2.8}$$

$$\Omega(R) = \left[\frac{2\epsilon'(5 + 2\epsilon')}{9\alpha^2} g(\alpha, \epsilon')\right]^{1/2} \frac{v_{\text{ff}}}{R}, \tag{2.9}$$

$$c_s^2(R) = \frac{2(5 + 2\epsilon')}{9\alpha^2} g(\alpha, \epsilon') v_{\text{ff}}, \tag{2.10}$$

where

$$v_{\text{ff}} \equiv \left(\frac{GM}{R}\right)^{1/2}, \quad \epsilon' \equiv \frac{\epsilon}{f} = \frac{1}{f}\left(\frac{5/3 - \gamma}{\gamma - 1}\right), \quad g(\alpha, \epsilon') \equiv \left[1 + \frac{18\alpha^2}{(5 + 2\epsilon')^2}\right]^{1/2} - 1. \tag{2.11}$$

γ is the ratio of specific heats of the gas, which is likely to lie in the range 4/3 to 5/3 (the two limits correspond to a radiation pressure–dominated and a gas pressure–dominated accretion flow, respectively). Correspondingly, ϵ lies in the range 0 to 1.

In general, f depends on the details of the heating and cooling and will vary with R. The assumption of a constant f is therefore an oversimplification. However, when the flow is highly advection dominated, $f \sim 1$ throughout the flow, and f can be well approximated as constant. Setting $f = 1$ and taking the limit $\alpha^2 \ll 1$ (which is nearly always true), the solution (2.8)–(2.10) takes the simple form

$$\frac{v}{v_{\text{ff}}} \simeq -\left(\frac{\gamma - 1}{\gamma - 5/9}\right)\alpha, \quad \frac{\Omega}{\Omega_K} \simeq \left[\frac{2(5/3 - \gamma)}{3(\gamma - 5/9)}\right]^{1/2}, \quad \frac{c_s^2}{v_{\text{ff}}^2} \simeq \frac{2}{3}\left(\frac{\gamma - 1}{\gamma - 5/9}\right). \tag{2.12}$$

A number of interesting features of ADAFs are revealed by the self–similar solution. (1) As we discuss below (§4.1.3), it appears that ADAFs have relatively large values of the viscosity parameter, $\alpha \gtrsim 0.1$; typically, $\alpha \sim 0.2 - 0.3$. This means that the radial velocity of the gas in an ADAF is comparable to the free–fall velocity, $v \gtrsim 0.1 v_{\text{ff}}$. The gas thus accretes quite rapidly. (2) The gas rotates with a sub–Keplerian angular velocity and is only partially supported by centrifugal forces. The rest of the support is from a radial pressure gradient, $\nabla P \sim \rho c_s^2/R \sim (0.3 - 0.4)v_{\text{ff}}^2/R$. In the extreme case when $\gamma \to 5/3$, the flow has no rotation at all ($\Omega \to 0$). (3) Since most of the viscously generated energy is stored in the gas as internal energy, rather than being radiated, the gas temperature is quite high; in fact, optically thin ADAFs have almost virial temperatures. This causes the gas to "puff up": $H \sim c_s/\Omega_K \sim v_{\text{ff}}/\Omega_K \sim R$.
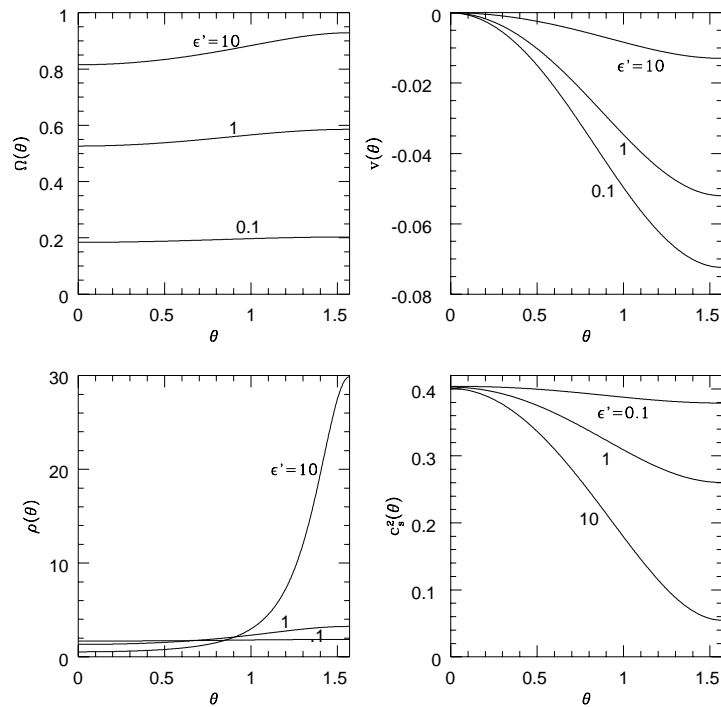
FIGURE 1. Angular profiles for radial self–similar solutions with $\alpha = 0.1$, $\epsilon' = 0.1, 1, 10$. *Top left:* angular velocity Ω/Ω_K as a function of polar angle θ. *Top right:* radial velocity, $v/v_{\rm ff}$. *Bottom left:* density, ρ. *Bottom right:* sound speed squared, $c_s^2/v_{\rm ff}^2$.

Therefore, geometrically, ADAFs resemble spherical Bondi (1952) accretion more than thin disk accretion. It is, however, important to note that the *dynamics* of ADAFs are very different from that of Bondi accretion (§2.7). (4) The gas flow in an ADAF has a positive Bernoulli parameter (Narayan & Yi 1994, 1995a), which means that if the gas were somehow to reverse its direction, it could reach infinity with net positive energy. This suggests a possible connection between ADAFs and jets. (5) The entropy of the gas increases with decreasing radius. ADAFs are therefore convectively unstable (Narayan & Yi 1994, 1995a; Igumenshchev, Chen, & Abramowicz 1996).

2.3. *Vertical Structure*

The quasi–spherical nature of the gas flow in an ADAF might indicate that the use of height integrated equations is an oversimplification. This led Narayan & Yi (1995a) to investigate the structure of ADAFs in the polar direction, θ. Making use of non–height–integrated equations, they searched for radially self–similar solutions; for example, they assumed that the density scales as $\rho \propto R^{-3/2}\rho(\theta)$, with a dimensionless function $\rho(\theta)$; the radial velocity scales as $v \propto R^{-1/2}v(\theta)$, etc.. The results confirmed that ADAFs are quasi–spherical and quite unlike thin disks.

Figure 1 shows the variation of Ω, v, ρ and c_s^2 as a function of θ for some typical solutions ($\alpha = 0.1$, $\epsilon' = 0.1, 1, 10$). For fully advection dominated flows ($f = 1$), different values of ϵ' correspond to different values of γ: the three solutions shown have $\gamma = 1.61, 1.33, 1.06$. If γ is fixed, than increasing ϵ' corresponds to decreasing f. Large values of ϵ' therefore correspond to cooling–dominated thin disk solutions whereas small values of ϵ' correspond

to highly advection–dominated flows. From Figure 1, we find that Ω, ρ and c_s^2 in ADAFs ($\epsilon' = 0.1, 1$) are nearly constant on radial shells. The radial velocity v is zero at the poles and reaches a maximum at the equator. Most of the accretion therefore takes place in the equatorial plane. The figure also shows the expected features of a thin disk in the limit of efficient cooling ($\epsilon' = 10$); the density is peaked near the equator, and Ω approaches Ω_K.

Despite the quasi–spherical nature of the flow, Narayan & Yi (1995a) found that the solutions of the exact non–height–integrated equations agree quite well with those of the simplified height–integrated equations (§2.2), provided that "height–integration" is done along θ at constant spherical radius, rather than along z at constant cylindrical radius. The height–integrated equations therefore are a fairly accurate representation of quasi–spherical ADAFs. (Technically, this has been proved only in the self-similar regime.)

2.4. *Pseudo–Newtonian Global Solutions*

The self–similar solution is scale free and does not match the boundary conditions of the flow. To proceed beyond self-similarity it is necessary to solve the full equations (2.1)–(2.4) with proper boundary conditions. For example, far from a central black hole, an ADAF might join on to a thin disk. At this radius, the rotational and radial velocities, as well as the gas density and sound speed, must take on values appropriate to a thin disk. Also, as the accreting gas flows in toward the black hole, it must undergo a sonic transition at some radius R_{sonic}, where the radial velocity equals the local sound speed. In addition, since the black hole cannot support a shear stress, the torque at the horizon must be zero, which is yet another boundary condition to be satisfied by the solutions. (Alternatively, if a causal viscosity prescription is used, there is a boundary condition at the causal horizon; see, e.g., Gammie & Popham (1998)) From the simple scalings of the self–similar solution (2.8)–(2.10), it is evident that the solution does not satisfy the boundary conditions and, therefore, is not a good approximation near the flow boundaries. In fact, the question arises: is the self–similar solution a good approximation to the global flow at any radius?

This question was investigated by Narayan, Kato, & Honma (1997a) and Chen, Abramowicz & Lasota (1997; see also Matsumoto et al. 1985; Abramowicz et al. 1988; Narayan & Yi 1994). Integrating the angular momentum equation (eq. [2.3]) once, one obtains

$$\frac{d\Omega}{dR} = \frac{v\Omega_K(\Omega R^2 - j)}{\alpha R^2 c_s^2}, \tag{2.13}$$

where the integration constant j is the angular momentum per unit mass accreted by the central mass. Recalling that eq. (2.1) integrates to give the constant mass accretion rate, $\dot{M}$, the global steady state problem consists of solving the differential equations (2.2), (2.4), and (2.13), along with proper boundary conditions, to obtain $v(R)$, $\Omega(R)$, $c_s(R)$, $\ln[\rho(R)]$, and the eigenvalue j.

Narayan et al. (1997a) and Chen et al. (1997) obtained global solutions for accretion on to a black hole, using a pseudo–Newtonian potential (Paczyński & Wiita 1980), with $\phi(R) = -GM/(R - R_S)$ and $\Omega_K^2 = GM/(R - R_S)^2 R$, which simulates a Schwarzschild black hole of radius $R_S = 2GM/c^2$. The global solutions agree quite well with the self-similar solutions, except near the boundaries, where there are significant deviations. This means that the self-similar solution provides a good approximation to the real solution over most of the flow.

Figure 2 shows the radial variation of the specific angular momentum and gas pressure in the inner regions of global ADAF solutions for several α. It is seen that low α ADAFs
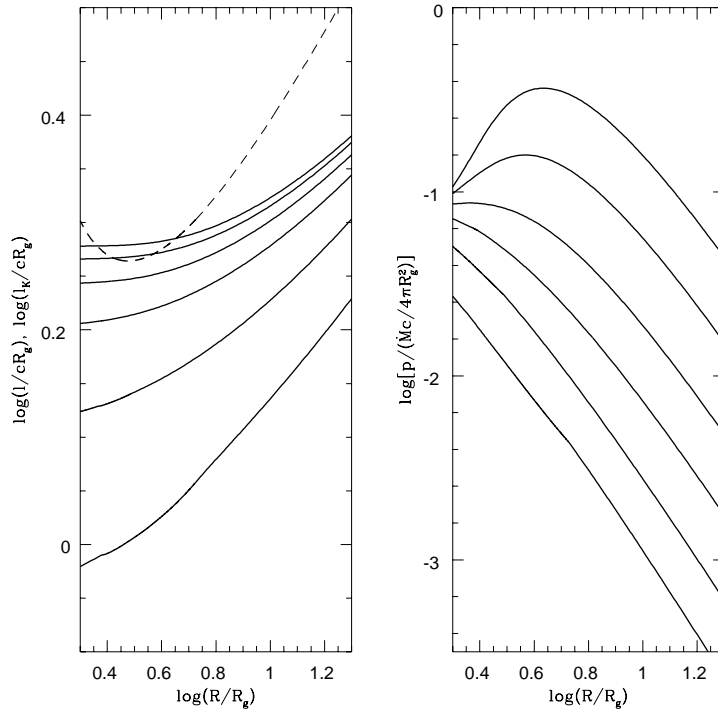
FIGURE 2.   *left*: Radial variation of the specific angular momentum, l, for (solid lines, from top to bottom) $\alpha = 0.001$, 0.003, 0.01, 0.03, 0.1, and 0.3. The dashed line shows the Keplerian specific angular momentum, l_K. Note that the low α solutions (0.001 and 0.003) are super-Keplerian ($l > l_K$) over a range of radii, whereas the solutions with larger α have $l < l_K$ for all radii. *right*: Radial variation of the gas pressure for the same α. Note that the low α curves (the two upper ones) have pressure maxima, associated with the super-Keplerian rotation shown in the left panel (taken from Narayan et al. 1997a).

are quite different from high α ADAFs, the division occurring at roughly $\alpha \sim 0.01$. When $\alpha \lesssim 0.01$, the gas in an ADAF is somewhat inefficient at transferring angular momentum outwards, has low radial velocity, and is nearly in hydrostatic equilibrium. The flow is super–Keplerian over a range of radii and has an inner edge near the marginally stable orbit (see fig. 2). The super–Keplerian flow creates a funnel along the rotation axis, which leads to a toroidal morphology. These solutions closely resemble the thick–torus models studied by Fishbone & Moncrief (1976), Abramowicz et al. (1978), Paczyński & Wiita (1980), and others (see Frank et al. 1992), and on which the ion torus model of Rees et al. (1982) is based.

When $\alpha \gtrsim 0.01$, on the other hand, the flow dynamics is dominated by viscosity, which efficiently removes angular momentum from the gas. The gas then has a large radial velocity, $v \sim \alpha v_{ff}$, remains sub–Keplerian at all radii, and has no pressure maximum outside the sonic radius. High α ADAFs therefore do not possess empty funnels and are unlikely to be toroidal in morphology. Instead the flow is probably quasi–spherical all the way down to the sonic radius; in fact, these ADAFs are more akin to slowly rotating settling stars, as illustrated in Fig. 3. As we discuss below (§4.1.3), two–temperature ADAFs have $\alpha \sim 0.2 - 0.3$, which places them firmly in the regime of quasi–spherical, rather than toroidal, flows.
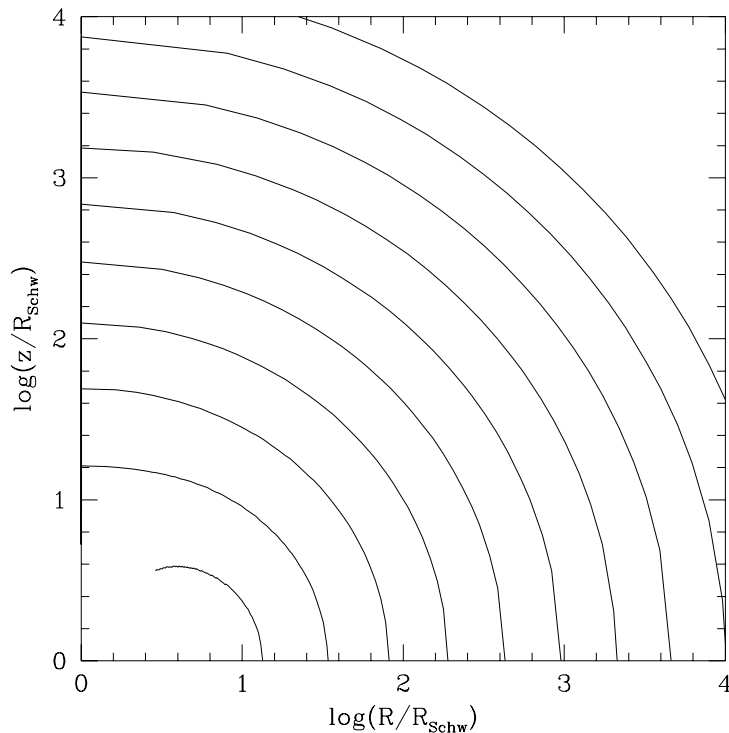
FIGURE 3. Isodensity contours (two contours per decade) in the $R-z$ plane for a global ADAF with $\alpha = 0.3$, $\gamma = 1.4444$ and $f = 1$. The contours are truncated at the sonic radius since the vertical structure is unreliable inside this radius. (Taken from Narayan 1997).

2.5. *Relativistic Global Solutions*

The global solutions described above are based on Newtonian physics. Recently, fully relativistic global solutions in the Kerr geometry have been calculated by Abramowicz et al. (1996), Peitz & Appl (1997) and Gammie & Popham (1998). Gammie & Popham (1997) find that their relativistic solutions are similar to the global solutions of Narayan et al. (1997a) for radii $R \gtrsim 10R_S$, while for $R \lesssim 10R_S$ the solutions differ significantly. They also show that, in the inner regions of the flow, the black hole's spin has a substantial effect on the density, temperature, angular momentum and radial velocity of the accreting gas. This is likely to have an impact on the observed spectrum (Jaroszyński & Kurpiewski 1997). A detailed survey of solutions for various parameters is discussed in Popham & Gammie (1998).

To summarize the last four subsections, a fairly advanced level of understanding has been achieved for the dynamics of ADAFs. There has been progress on two fronts. First, the two-dimensional structure of the flow in $R-\theta$ is understood in the radially self-similar regime. Second, using height-integration (which is shown to be an excellent approximation in the self-similar zone), the radial structure of the flow, including the effects of boundary conditions, has been worked out including full general relativity. Several problems, however, remain. The two-dimensional structure in the boundary regions, where the flow deviates substantially from self-similarity, is not understood. There may be solutions that are qualitatively distinct from the ones discovered so far, e.g., solutions with jets. In addition, three dimensional effects may arise from spiral modes, convective

turbulence, etc.. Finally, the introduction of MHD effects in the fluid equations may reveal new phenomena which go beyond the hydrodynamic approximations considered so far.

2.6. *On the Possibility of Radial Shocks*

The global steady state solutions discussed in §2.4 and §2.5 are free of radial shocks. Igumenshchev et al. (1997) have carried out time–dependent simulations of global transonic flows and again find no shocks. However, Chakrabarti and his collaborators (see Chakrabarti 1996 for a review of this work) have claimed that shocks are generic to ADAFs. The clearest statement of his results is found in Chakrabarti & Titarchuk (1995); the authors claim: (i) Low α ($\lesssim 0.01$) flows have shocks and high α ($\gtrsim 0.01$) flows do not. (ii) Low α flows have sub–Keplerian rotation at large radii while high α flows are Keplerian at all radii except very close to the black hole. Neither statement has been confirmed by other workers. In particular, no shocks are seen in any of the global solutions, which span a wide range of parameter values: α ranging from 10^{-3} to 0.3, and γ from 4/3 to 5/3. The reader is referred to Narayan et al. (1997a) and Narayan (1997) for a more detailed discussion of the lack of radial shocks in ADAF solutions.

2.7. *ADAFs versus Pure Spherical Accretion*

Geometrically, ADAFs are similar to spherical Bondi accretion. They are quasi–spherical and have radial velocities which are close to free fall, at least for large α. Also, the gas passes through a sonic radius and falls supersonically into the black hole.

Despite these similarities, it is important to stress that ADAFs are *dynamically* very different from pure spherical accretion. Transport of angular momentum through viscosity plays a crucial role in ADAFs; indeed, there would be no accretion at all without viscosity (recall that $v \propto \alpha$, cf. eq. [2.12]). Bondi accretion, on the other hand, involves only a competition between inward gravity and outward pressure gradient; viscosity plays no role.

In the Bondi solution, the location of the sonic radius is determined by the properties of the accreting gas at large radii. Under many conditions, the sonic radius is quite far from the black hole. In an ADAF, on the other hand, the sonic radius is almost always at a few R_S. Furthermore, the location of the sonic radius depends on the viscosity parameter α (another indication of the importance of viscosity) and the properties of the gas at infinity are irrelevant so long as the gas has enough angular momentum to prevent direct radial infall. In addition, the gas temperature, or energy density, in an ADAF is determined by viscous heating and adiabatic compression, and is generally much higher than in Bondi accretion. Also, the rotational velocities in ADAFs are quite large, reaching nearly virial velocities, whereas Ω is strictly zero in the Bondi solution.

In nature, when gas accretes onto a black hole, it nearly always has too much angular momentum to fall directly into the hole. ADAFs are, therefore, much more relevant than the Bondi solution for the description of accretion flows around black holes.

3. Two–Temperature ADAFs

As mentioned in §1, two types of ADAFs are known, a high–$\dot{M}$ optically thick solution and a low–$\dot{M}$ optically–thin, two–temperature solution. The high–$\dot{M}$ ADAF, though well–understood dynamically, has seen few applications to observations. In particular, the spectral properties of this solution have not been studied in detail (see, however, Szuszkiewicz et al. 1996 for a recent study). In contrast, the low–$\dot{M}$ ADAF has been extensively studied during the last few years and has been widely applied to black hole

X–ray binaries and low–luminosity galactic nuclei. The rest of this article is devoted to this solution.

The two-temperature ADAF solution (though not by this name) was first described in a remarkable paper by Ichimaru (1977). This paper clearly distinguished the ADAF solution from the SLE solution and argued (without proof) that the ADAF solution would be stable. It also suggested that the black hole X-ray binary Cyg X-1, in its so called low state (the hardest spectrum in Fig. 14), corresponds to an ADAF. Unfortunately, this paper was soon forgotten; in fact, its very existence was unknown to later generations of disk theorists until the paper was rediscovered and brought to the attention of the community by Roland Svensson at the present workshop.

Elements of the two-temperature ADAF were described independently by Rees et al. (1982) in their "ion torus" model. This paper, however, though not forgotten, did not have a strong influence on later workers. Indeed, all through the 1980's and the early half of the 1990's, the SLE solution was studied in greater detail than the ion torus model. (Even Svensson did most of his work on the SLE solution!) It appears that most scientists in the community did not recognize that the SLE solution and the ion torus model were distinct, and even those that did were not fully aware of their different stability properties.

The current interest in the two-temperature ADAF solution was initiated by the papers of Narayan & Yi (1994, 1995a, 1995b), Abramowicz et al. (1995), Chen (1995), Chen et al. (1995), and a host of others. These workers discovered the solution for the third time, but this time developed it in considerable detail, studied its properties, and applied it widely to a number of systems.

3.1. *Basic Assumptions*

Models based on the two–temperature ADAF solution make certain critical assumptions. The validity of these assumptions is not proved and is currently under investigation.

3.1.1. *Equipartition Magnetic Fields*

It is assumed that magnetic fields contribute a constant fraction $(1 - \beta)$ of the total pressure:

$$p_{\mathrm{m}} = \frac{B^2}{24\pi} = (1 - \beta)\rho c_s^2, \qquad (3.14)$$

where p_{m} is the magnetic pressure due to an isotropically tangled magnetic field. Note that the usual β of plasma physics is related to the β utilized here by $\beta_{\mathrm{plasma}} = \beta/3(1-\beta)$ (the $1/3$ arises because the plasma β uses $B^2/8\pi$ for the magnetic pressure, rather than $B^2/24\pi$). The assumption of a constant β is fairly innocuous since, in general, we expect equipartition magnetic fields in most astrophysical plasmas. In particular, Balbus & Hawley (1991) have shown that differentially rotating disks with weak magnetic fields develop a strong linear MHD instability which exponentially increases the field strength to near equipartition values. The exact saturation value of p_{m} is, however, unclear (e.g., Hawley, Gammie, & Balbus 1996). ADAF models assume $\beta = 0.5$ (or $\beta_{\mathrm{plasma}} = 1/3$), i.e., strict equipartition between gas and (tangled) magnetic pressure. The presence of equipartition magnetic fields implies that the effective adiabatic index in the energy equation is not that of a monatomic ideal gas. Esin (1997) argues that the appropriate expression is $\gamma = (8 - 3\beta)/(6 - 3\beta)$.

3.1.2. *Thermal Coupling Between Ions and Electrons*

ADAF models assume that ions and electrons interact only through Coulomb collisions and that there is no non–thermal coupling between the two species. In this case the

plasma is two temperature, with the ions much hotter than the electrons. This important assumption may be questioned on the grounds that magnetized collisionless plasmas, such as ADAFs, have many modes of interaction; intuitively, it would seem that the plasma might be able to find a more efficient way than Coulomb collisions of exchanging energy between the ions and the electrons (Phinney 1981). To date, however, only one potential mechanism has been identified. Begelman & Chiueh (1989) show that, under appropriate conditions, large ion drift velocities (due to significant levels of small scale turbulence in the accretion flow) may drive certain plasma waves unstable, which then transfer energy directly from the ions to the electrons. Narayan & Yi (1995b), however, argue that for most situations of interest, the specific mechanism identified by Begelman & Chiueh (1989) is not important for ADAF models.

3.1.3. *Preferential Heating of Ions*

The two-temperature ADAF model assumes that most of the turbulent viscous energy goes into the ions (SLE; Ichimaru 1977; Rees et al. 1982; Narayan & Yi 1995b), and that only a small fraction $\delta \ll 1$ goes into the electrons. The parameter δ is generally set to $\sim 10^{-3} \sim m_e/m_p$, but none of the results depend critically on the actual value of δ, so long as it is less than a few percent. Recently, there have been several theoretical investigations which consider the question of particle heating in ADAFs.

Bisnovatyi–Kogan & Lovelace (1997) argue that large electric fields parallel to the local magnetic field preferentially accelerate electrons (by virtue of their smaller mass), leading to $\delta \sim 1$. In magnetohydrodynamics (MHD), however, an electric field parallel to the magnetic field arises only from finite resistivity effects and is of order $\sim vB/c\mathrm{Re_m}$, where $\mathrm{Re_m} \gg 1$ is the magnetic Reynolds number. Local parallel electric fields are therefore negligible. Bisnovatyi–Kogan & Lovelace (1997) suggest that, instead of the microscopic resistivity, one must use the macroscopic or turbulent resistivity to determine the local electric field, in which case parallel electric fields are large, $\sim vB/c$. The problem with this analysis, as discussed by Blackman (1998) and Quataert (1998), is that the turbulent resistivity is defined only for the large scale (mean) fields. On small scales, the MHD result mentioned above is applicable and so parallel electric fields are unimportant for accelerating particles.

Blackman (1998), Gruzinov (1998), and Quataert (1998) consider particle heating by MHD turbulence in ADAFs. Blackman shows that Fermi acceleration by large scale magnetic fluctuations associated with MHD turbulence preferentially heats the ions in two temperature, gas pressure dominated, plasmas. This is, however, equivalent to considering the collisionless damping of the fast mode component of MHD turbulence (Achterberg 1981), and thus does not apply to the non-compressive, i.e., Alfvenic, component (which is likely to be energetically as or more important than the compressive component).

Following the work of Goldreich & Sridhar (1995) on Alfvenic turbulence, Gruzinov (1998) and Quataert (1998) show that, when the magnetic field is relatively weak, the Alfvenic component of MHD turbulence is dissipated on length scales of order the proton Larmor radius. The damping is primarily by "magnetic" Landau damping (also known as transit time damping, Cherenkov damping, etc.), not the cyclotron resonance (which is unimportant), and most of the Alfvenic energy heats the ions rather than the electrons. For equipartition magnetic fields, Gruzinov argues that Alfvenic turbulence will cascade to length scales much smaller than the proton Larmor radius and heat the electrons. An extension of this work is given in Quataert & Gruzinov (1998).

3.1.4. α Viscosity

The viscosity parameter α of Shakura & Sunyaev (1973) is used to described angular momentum transport; α is assumed to be constant, independent of radius. Some authors have proposed that α may vary as a function of (H/R). Since ADAFs have $H \sim R$, no radial dependence is expected, and a constant α appears to be a particularly good assumption (Narayan 1996b). Since the viscous stress is probably caused by magnetic fields, the parameters α and β are likely to be related according to the prescription of Hawley, Gammie & Balbus (1996): $\alpha = 3c(1 - \beta)/(3 - 2\beta)$, where $c \sim 0.5 - 0.6$. This expression for $\alpha(\beta)$ differs from the expression given elsewhere in the literature (e.g., Narayan et al. 1998), $\alpha = c(1 - \beta)$, in properly recognizing that Hawley et al. define magnetic pressure as $B^2/8\pi$, while we use equation (3.14). For equipartition magnetic fields ($\beta = 0.5$), $\alpha \sim 0.4$. The models in the literature usually set α to 0.25 or 0.3.

3.2. Properties of Two–Temperature, Optically Thin, ADAFs

For the remainder of this review, we write all quantities in scaled units: the mass is scaled in solar mass units,

$$M = mM_\odot,$$

the radius in Schwarzschild radii,

$$R = rR_S, \qquad R_S = \frac{2GM}{c^2} = 2.95 \times 10^5 m \quad \text{cm},$$

and the accretion rate in Eddington units,

$$\dot{M} = \dot{m}\,\dot{M}_{\text{Edd}}, \quad \dot{M}_{\text{Edd}} = \frac{L_{\text{Edd}}}{\eta_{\text{eff}}c^2} = 1.39 \times 10^{18}\, m \quad \text{g s}^{-1},$$

where we have set η_{eff}, the efficiency of converting matter to radiation, equal to 0.1 in the definition of $\dot{M}_{\text{Edd}}$ (cf. Frank et al. 1992).

3.2.1. Scaling Laws

Using the self–similar solution (2.8)–(2.10), one can obtain a fairly good idea of the scalings of various quantities in an ADAF as a function of the model parameters. Setting $f \to 1$ (advection–dominated flow) and $\beta = 0.5$ (equipartition magnetic field), one finds (Narayan & Yi 1995b; see also Mahadevan 1997),

$$v \simeq -1.1 \times 10^{10}\, \alpha r^{-1/2} \quad \text{cm s}^{-1},$$

$$\Omega \simeq 2.9 \times 10^4\, m^{-1} r^{-3/2} \quad \text{s},$$

$$c_s^2 \simeq 1.4 \times 10^{20}\, r^{-1} \quad \text{cm}^2 \text{ s}^{-2},$$

$$n_e \simeq 6.3 \times 10^{19}\, \alpha^{-1} m^{-1} \dot{m}\, r^{-3/2} \quad \text{cm}^{-3},$$

$$B \simeq 7.8 \times 10^8\, \alpha^{-1/2} m^{-1/2} \dot{m}^{1/2}\, r^{-5/4} \quad \text{G},$$

$$p \simeq 1.7 \times 10^{16}\, \alpha^{-1} m^{-1} \dot{m}\, r^{-5/2} \quad \text{g cm}^{-1} \text{ s}^{-2},$$

$$q^+ \simeq 5.0 \times 10^{21}\, m^{-2} \dot{m}\, r^{-4} \quad \text{ergs cm}^{-3} \text{ s}^{-1},$$

$$\tau_{\text{es}} \simeq 24\, \alpha^{-1} \dot{m}\, r^{-1/2}, \tag{3.15}$$

where n_e is the electron density, p is the pressure (gas plux magnetic), and τ_{es} is the electron scattering optical depth to infinity.

3.2.2. *Critical Mass Accretion Rate*

The optically thin ADAF solution exists only for $\dot{m}$ less than a critical value $\dot{m}_{\rm crit}$ (Ichimaru 1977; Rees et al. 1982; Narayan & Yi 1995b; Abramowicz et al. 1995; Esin et al. 1996, 1997). To derive this result, consider first an optically thin one–temperature gas which cools primarily by free–free emission (Abramowicz et al. 1995). This is a reasonable model at large radii, $r > 10^3$. The viscous heating rate varies as $q^+ \propto m^{-2}\dot{m}r^{-4}$ (eq. 3.15), while the cooling varies as $q^- \propto n_p n_e T_e^{1/2} \propto \alpha^{-2} m^{-2} \dot{m}^2 T_e^{1/2} r^{-3}$, where n_p is the proton number density. For a one–temperature ADAF, $T_e \sim m_p c_s^2/k \sim 10^{12}{\rm K}/r$, and is independent of $\dot{m}$. By comparing q^+ and q^-, it is easily seen that there is an $\dot{m}_{\rm crit} \propto \alpha^2 r^{-1/2}$, such that for $\dot{m} < \dot{m}_{\rm crit}$, we have $q^+ > q^-$ and a consistent ADAF solution, whereas for $\dot{m} > \dot{m}_{\rm crit}$ no ADAF is possible. Note that $\dot{m}_{\rm crit}$ decreases with increasing r. The decrease is as $r^{-1/2}$ if the cooling is dominated by free–free emission. If other atomic cooling processes are also included, the decrease is more rapid (cf. Fig. 8).

The above argument assumes free–free cooling, which is the dominant cooling mechanism at non–relativistic temperatures. However, once electrons become relativistic, other cooling processes such as synchrotron radiation and inverse Compton scattering take over. Esin et al. (1996) showed that even in this situation it is possible to have a one-temperature ADAF at sufficiently low $\dot{m}$. However, the critical accretion rate $\dot{m}_{\rm crit}$ is very small, $\sim 10^{-6}$ (for $\alpha \approx 0.25$; Esin et al. found $\dot{m}_{\rm crit} \sim 10^{-4}\alpha^2$, but more detailed calculations give a somewhat smaller value). Models with such low mass accretion rates are not of much interest for modeling observed systems.

If we allow a two–temperature plasma, then the ADAF solution can, utilizing the assumptions given in the previous subsections, extend up to larger and more interesting mass accretion rates (Ichimaru 1977; Rees et al. 1982; Narayan & Yi 1995b). By assumption, the viscous energy primarily heats the protons, while the cooling is almost entirely by the electrons. At low densities Coulomb coupling between protons and electrons is very weak and the amount of viscous energy that is transferred to the electrons is very small. Coulomb coupling therefore acts as a bottleneck which restricts the amount of energy that can be lost to radiation.

With increasing $\dot{m}$, Coulomb coupling becomes more efficient, and at a critical density the coupling is so efficient that a large fraction of the viscous energy is transferred to the electrons and is radiated. Above this accretion rate, the flow ceases to be an ADAF; it becomes a standard cooling–dominated thin disk. The critical accretion rate can be estimated by determining the $\dot{m}$ at which the viscous heating, q^+, equals the rate of energy transfer from the ions to the electrons, $q^{\rm ie}$. Alternatively, we can set the ion–electron equilibration time (the time for collisions to force $T_i \approx T_e$), $t_{\rm ie}$, equal to the accretion time, $t_{\rm a}$. The former time scale is given by (Spitzer 1962)

$$t_{\rm ie} = \frac{(2\pi)^{1/2}}{2\,n_e \sigma_T c \ln \Lambda} \left(\frac{m_p}{m_e}\right) (\theta_e + \theta_p)^{3/2},$$

$$\simeq 9.3 \times 10^{-5} \alpha\, \theta_e^{3/2}\, m\, \dot{m}^{-1}\, r^{3/2} \quad {\rm s},$$

where $\ln \Lambda \sim 20$ is the Coulomb logarithm, $\theta_p = kT_p/m_p c^2$, and $\theta_e = kT_e/m_e c^2$. The accretion time is given by

$$t_{\rm a} = \int \frac{dR}{v(R)} \simeq 1.8 \times 10^{-5}\, \alpha^{-1}\, m\, r^{3/2} \quad {\rm s}. \tag{3.16}$$

Setting these two timescales equal gives

$$\dot{m}_{\rm crit} \simeq 5\theta_e^{3/2}\alpha^2 \simeq 0.3\alpha^2, \tag{3.17}$$

where we have used $\theta_e \sim 0.16$, corresponding to $T_e = 10^9$K (Mahadevan 1997). More detailed models (cf. Esin et al. 1997) give $\dot{m}_{\rm crit} \sim \alpha^2$. This value of $\dot{m}_{\rm crit}$ is essentially independent of r out to about $10^2 - 10^3$ Schwarzschild radii. Beyond that, the accreting gas becomes one-temperature and $\dot{m}_{\rm crit}$ decreases with increasing r, as explained above. Figure (8) shows a detailed estimate of the profile of $\dot{m}_{\rm crit}$ vs r. In this review, we will refer to the full profile as $\dot{m}_{\rm crit}(r)$ and refer to $\dot{m}_{\rm crit}(r_{ms})$ as simply $\dot{m}_{\rm crit}$, where r_{ms} is the marginally stable orbit ($r_{ms} = 3$). Thus, $\dot{m}_{\rm crit}$ refers to the maximum $\dot{m}$ up to which an ADAF zone of any size is allowed.

As we discuss later, observations suggest that the two–temperature ADAF solution exists up to $\dot{m}_{\rm crit} \sim 0.05 - 0.1$. This suggests that $\alpha \sim 0.2 - 0.3$ in ADAFs.

3.2.3. *Temperature Profiles of Ions and Electrons*

In a two–temperature ADAF the ions receive most of the viscous energy and are nearly virial (Narayan & Yi 1995b),

$$T_i \simeq 2 \times 10^{12} \beta r^{-1}.$$

The electrons, on the other hand, are heated by several processes with varying efficiencies — Coulomb coupling with the ions, compression, and direct viscous heating (described by the parameter δ) — and cooled by a variety of radiation processes.

To determine the electron temperature profile, consider the electron energy equation (Nakamura et al. 1996, 1997; Mahadevan & Quataert 1997),

$$\rho T_e v \frac{ds}{dR} = \rho v \frac{d\epsilon}{dR} - q^c = q^{ie} + q^v - q^-, \qquad q^c \equiv kTv\frac{dn}{dR}, \qquad (3.18)$$

where s and ϵ are the entropy and internal energy of the electrons per unit mass of the gas, and q^c and q^- are the compressive heating (or cooling) rate and the energy loss due to radiative cooling per unit volume. The total heating rate of the electrons is the sum of the heating via Coulomb collisions with the hotter protons, q^{ie}, and direct viscous heating, $q^v = \delta q^+$. (Recall that δ is usually assumed to be $\sim 10^{-3}$ in ADAF models.)

The electron temperature at radii $r \lesssim 10^2$ in two–temperature ADAFs is generally in the range $10^9 - 10^{10}$K. The exact form of the electron temperature profile depends on which of the three heating terms dominates. Nakamura et al. (1996, 1997) were the first to emphasize the compressive heating term, q^c. Mahadevan & Quataert (1997) showed that compressive heating of the electrons is more important than direct viscous heating so long as $\delta \lesssim 10^{-2}$. Since $\delta \sim 10^{-3}$ in most models, we can ignore direct viscous heating and consider only the following two limits.

$q^{ie} \gg q^c$: This condition is satisfied for $\dot{m} \gtrsim 0.1\alpha^2$. Rewriting equation (3.18) in this regime gives

$$\rho v \frac{d\epsilon}{dR} \simeq q^{ie} + q^c - q^- \simeq q^{ie} - q^-.$$

Since the cooling is efficient enough to radiate away all of the energy given to the electrons, $q^{ie} = q^-$ for $r \lesssim 10^2$, and the internal energy of the electrons does not change with radius, $d\epsilon/dR = 0$. The electron temperature therefore remains essentially constant at $\sim 10^9$K (e.g. Narayan & Yi 1995b). The value of T_e depends weakly on $\dot{m}$ (Fig. 4).

$q^c \gg q^{ie}$: This condition is satisfied for $\dot{m} \lesssim 10^{-4}\alpha^2$. Rewriting equation (3.18) in this regime gives

$$\rho v \frac{d\epsilon}{dR} \simeq q^c + q^{ie} - q^- \simeq q^c.$$

The radial dependence of the electron temperature is determined by adiabatic compression (Nakamura et al. 1997; Mahadevan & Quataert 1997). The electron temperatures in this regime are slightly higher.
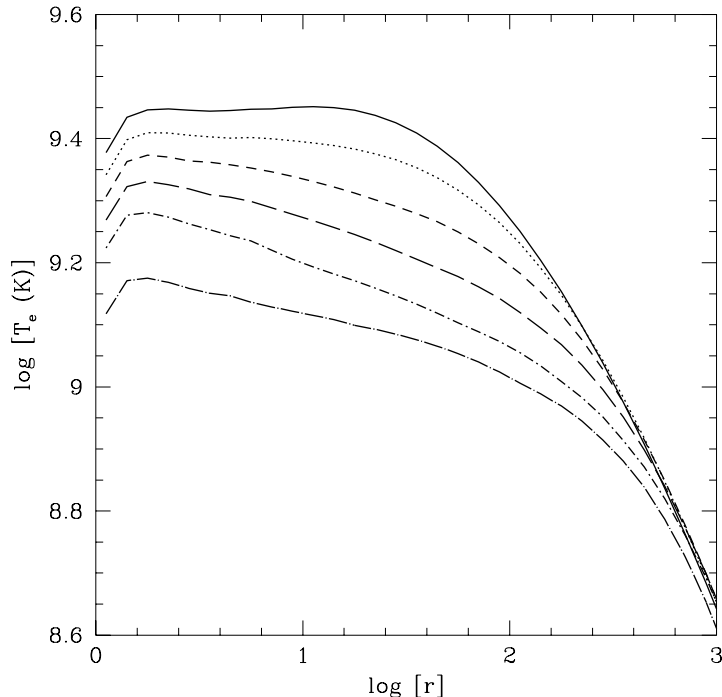
FIGURE 4. Variation of electron temperature T_e with radius r for ADAFs with (from top to bottom) $\log(\dot{m}) = -2, -1.8, -1.6, -1.4, -1.2, -1.1$ (taken from Esin et al. 1997). Note that the electron temperature decreases with increasing $\dot{m}$.

For $10^{-4}\alpha^2 \leq \dot{m} \leq 0.1\alpha^2$, the electron temperature profile lies in between these two extremes, and is determined by solving equation (3.18) without neglecting any of the heating terms.

Figure 4 shows the temperature profile as a function of radius for various $\dot{m}$. The electrons actually become cooler as the accretion rate increases. Since with increasing $\dot{m}$ the energy transferred to the electrons goes up, one might naively expect the electrons to reach higher temperatures in order to radiate the additional energy. In fact, the opposite happens; at high $\dot{m}$, the dominant cooling mechanism is inverse Compton scattering. This is an extremely efficient process when the optical depth approaches unity and its efficiency increases sharply with increasing optical depth, i.e., increasing $\dot{m}$.

Although the electrons achieve relativistic temperatures, pair processes are found to be unimportant in two-temperature ADAFs (Kusunose & Mineshige 1996, Björnsson et al. 1996, Esin et al. 1997). The reason is the low density, which allows very few pair-producing interactions in the medium.

3.2.4. *ADAF Spectra and Radiation Processes*

The spectrum from an ADAF around a black hole ranges from radio frequencies $\sim 10^9$Hz to gamma–ray frequencies $\gtrsim 10^{23}$Hz, and can be divided into two parts based on the emitting particles: (1) The radio to hard X–ray radiation is produced by electrons via synchrotron, bremsstrahlung and inverse Compton processes (Mahadevan 1997). (2) The gamma–ray radiation results from the decay of neutral pions created in proton–
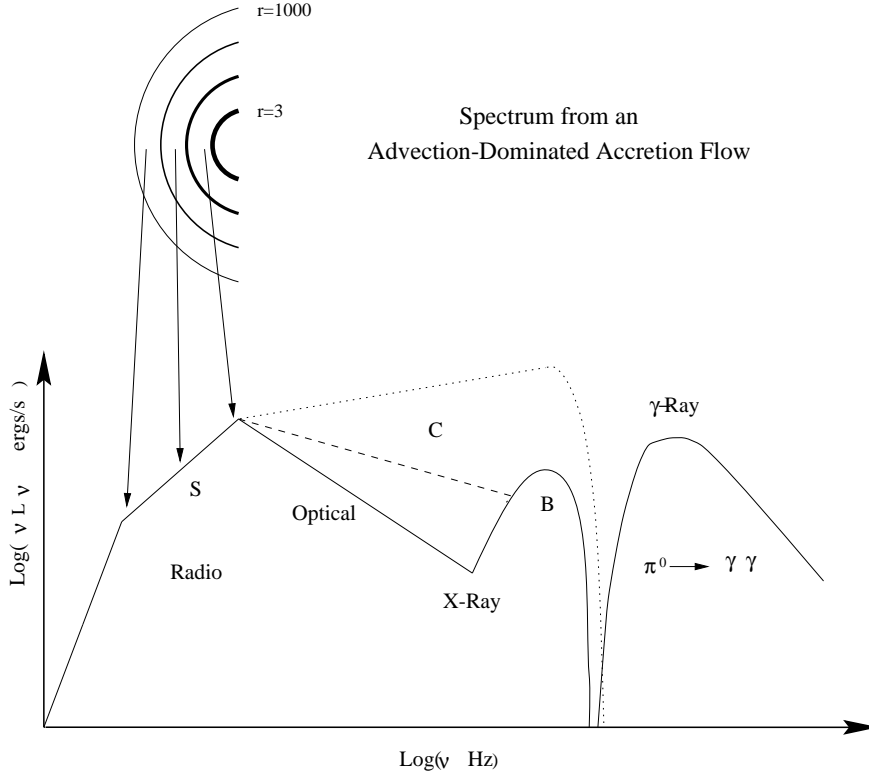
FIGURE 5. Schematic spectrum of an ADAF around a black hole. S, C, and B refer to electron emission by synchrotron radiation, inverse Compton scattering, and bremsstrahlung, respectively. The solid line corresponds to a low $\dot{m}$, the dashed line to an intermediate $\dot{m}$, and the dotted line to a high $\dot{m} \sim \dot{m}_{\rm crit}$. The γ–ray spectrum is due to the decay of neutral pions created in proton-proton collisions.

proton collisions (Mahadevan, Narayan & Krolik 1997). Figure (5) shows schematically the various elements in the spectrum of an ADAF around a black hole.

The low energy end of the spectrum, labeled S in the figure, is due to synchrotron cooling by semi–relativistic thermal electrons (Mahadevan et al. 1996). The synchrotron emission is highly self–absorbed and is very sensitive to the electron temperature ($\nu L_\nu \propto T_e^7$; Mahadevan 1997). The emission at the highest (peak) frequency comes from near the black hole, while that at lower frequencies comes from further out. The peak frequency varies with the mass of the black hole and the accretion rate, roughly as $\nu_{\rm peak}^S \propto m^{-1/2} \dot{m}^{1/2}$ (Mahadevan 1997; see figure 6).

The soft synchrotron photons inverse Compton scatter off the hot electrons in the ADAF and produce harder radiation extending up to about the electron temperature $\sim$ 100 keV ($h\nu_{\rm max}^C \approx kT_e$). The relative importance of this process depends on the mass accretion rate. At high $\dot{m}$, when the Compton y-parameter is large (because of the increased optical depth), the inverse Compton component dominates the spectrum, as shown by the dotted line labeled C in figure (5).

As $\dot{m}$ decreases, Comptonization becomes less efficient and the inverse Compton component of the spectrum becomes softer and less important (dashed and solid lines labeled C in figure 5). At low $\dot{m}$, the X–ray spectrum is dominated by bremsstrahlung emission, which again cuts off at the electron temperature ($h\nu_{\rm max}^B \approx kT_e$, the curve labeled B in figure 5).
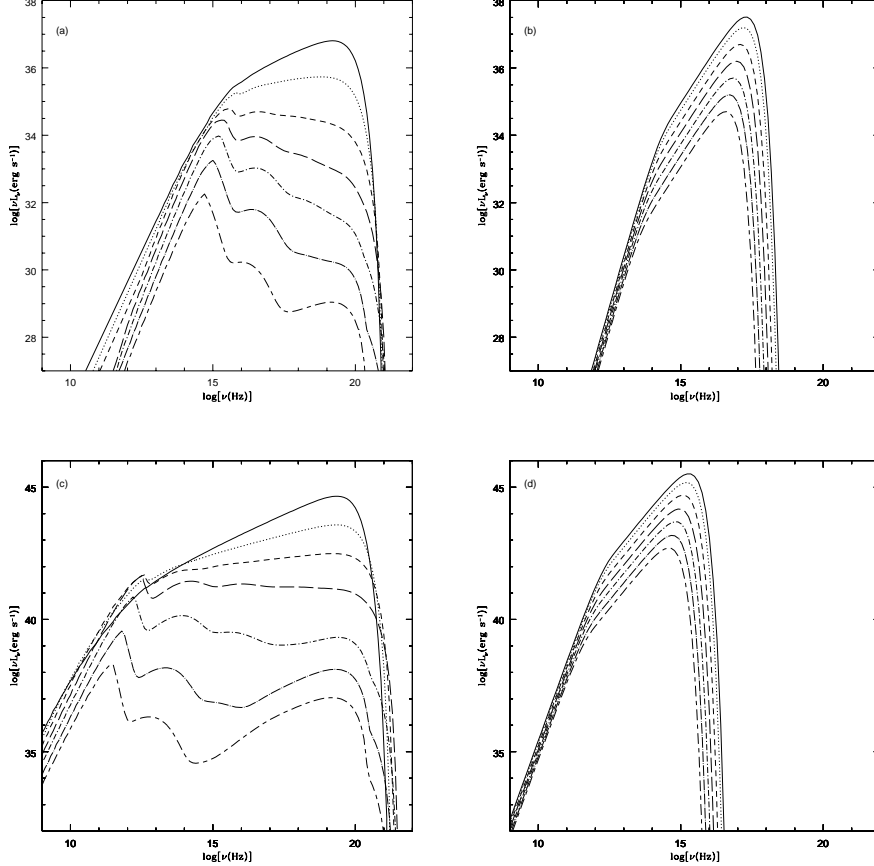
FIGURE 6. (a) Spectra from an ADAF around a 10 solar mass black hole for (from top to bottom) $\log(\dot{m}) = \log(\dot{m}_{\mathrm{crit}}) \approx -1.1, -1.5, -2, -2.5, -3, -3.5, -4$. (b) Spectra from a thin disk at the same accretion rates. Figures (c) and (d) show the corresponding spectra for a 10^9 solar mass black hole. Note that these spectra are for pure disk and pure ADAF models. In practice, real systems are often modeled as an ADAF surrounded by a thin disk (see §3.3). In such composite models, the ADAF part of the spectrum is essentially unchanged, but a dimmer and softer version of the thin disk is also present in the spectrum.

Mahadevan et al. (1997) have studied gamma-ray emission from an ADAF via the decay of neutral pions produced in proton-proton collisions. The results depend sensitively on the energy spectrum of the protons. If the protons have a thermal distribution, the gamma-ray spectrum is sharply peaked at ~ 70 MeV, half the rest mass of the pion, and the luminosity is not very high. If the protons have a power–law distribution, the gamma-ray spectrum is a power–law extending to very high energies (see figure 5), and the luminosity is much higher; the photon index of the spectrum is equal to the power–law index of the proton distribution function.

Figure (6) shows four sequences of spectra, two corresponding to ADAFs (excluding the gamma-ray component) and two to thin disks. Figures (6a) and (6b) are for a 10 solar mass black hole while Figures (6c) and (6d) are for a 10^9 solar mass black hole. All sequences extend over the same range of $\dot{m} = 10^{-4} - 10^{-1.1} \approx \dot{m}_{\mathrm{crit}}$. Note how very different the thin disk and ADAF spectra are, suggesting that it should be easy to tell from spectral observations whether a system has an ADAF or a thin disk.
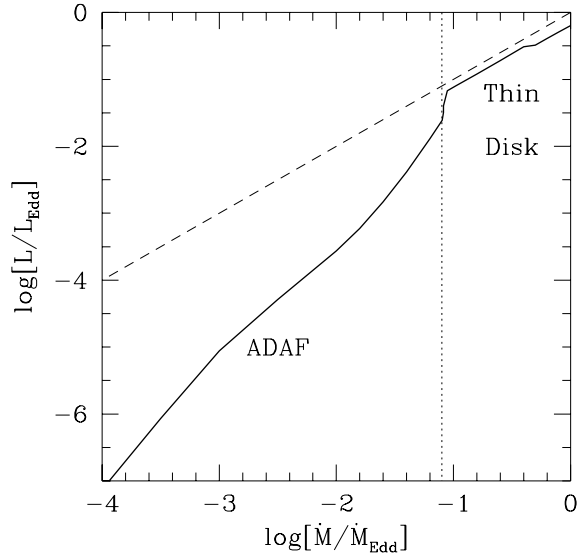
FIGURE 7. The bolometric luminosity vs. mass accretion rate according to the model developed by Esin et al. (1997). The vertical dotted line corresponds to $\dot{m}_{\mathrm{crit}}$ (for $\alpha = 0.3$). Above this $\dot{m}$, the accretion is via a thin disk and $L \propto \dot{M}$. Below $\dot{m}_{\mathrm{crit}}$, the accretion is via an ADAF at small radii and a thin disk at large radii (cf. §3.3). Here $L \propto \dot{M}^2$ because much of the viscously generated energy is advected into the black hole. The dashed line corresponds to $L = 0.1\dot{M}c^2$.

Figure (6) shows that for high $\dot{m}$, the Compton component of an ADAF spectrum is roughly a power law while for lower $\dot{m}$ distinct Compton peaks are present. This is primarily due to the increase of the electron temperature with decreasing $\dot{m}$ (see fig. 4). A larger T_e yields a larger energy boost per Compton scattering.. At low $\dot{m}$, the energy gain due to Compton scattering exceeds the width (in energy) of the input synchrotron photons, resulting in distinct Compton peaks. For increasing $\dot{m}$, however, T_e, and thus the mean energy gain due to Compton scattering, decreases. The Compton peaks therefore "blur" together, yielding an effective power law.

Another striking feature seen in Fig. (6) is that ADAFs are much less luminous than thin disks at low values of $\dot{m}$. This is because most of the energy in an ADAF is advected, rather than radiated, leading to a low radiative efficiency. In fact, the luminosity of an ADAF scales roughly as $\sim \dot{m}^2$ (i.e., the radiative efficiency scales as $\dot{m}$). A thin disk, on the other hand, has a constant efficiency $\sim 10\%$ and the luminosity scales as $\dot{m}$. This is illustrated in Fig. (7) which shows results of a detailed model described by Esin et al. (1997).

3.2.5. *The Particle Distribution Function in ADAFs*

In determining the radiation processes in ADAFs, the electrons are assumed to be thermal, while the protons could be thermal or non–thermal. It is clear that the spectrum will depend significantly on the energy distribution of the particles.

Mahadevan & Quataert (1997) considered two possible thermalization processes in ADAFs: (1) Coulomb collisions and (2) synchrotron self–absorption. Using an analytic Fokker–Planck treatment, they compared the time scales for these processes with the accretion time, and determined the accretion rates at which thermalization is possible. In the case of the protons they found that, for all accretion rates of interest, neither Coulomb collisions nor synchrotron self-absorption leads to any significant thermalization. The proton distribution function is therefore determined principally by the characteristics of the viscous heating mechanism, and could therefore be thermal or non–thermal. Quataert (1998) has argued that Alfvenic turbulence does *not* lead to strong non-thermal features in the proton distribution function; fast mode turbulence (Fermi acceleration), however, may generate a power-law tail.

The electrons exchange energy quite efficiently by Coulomb collisions for $\dot{m} \gtrsim 10^{-2}\alpha^2$, and are therefore thermal at these accretion rates. At lower $\dot{m}$ the emission and absorption of synchrotron photons allows the electrons to communicate with one another, and therefore to thermalize, even though the plasma is effectively collisionless (Ghisellini & Svensson 1990, 1991). At a radius r in the accretion flow, this leads to thermalization for $\dot{m} \gtrsim 10^{-5}\alpha^2 r$ (Mahadevan & Quataert 1997). For still lower $\dot{m}$, the electron distribution function is somewhat indeterminate, and is strongly influenced by adiabatic compression (Mahadevan & Quataert 1997). Detailed spectra of ADAFs at such low $\dot{m}$, which take into account the nonthermal distribution function of the electrons, have not been calculated (see, however, Fujita et al. (1998) for preliminary models of isolated black holes accreting at very low $\dot{m}$ from the interstellar medium).

3.2.6. *Stability of the ADAF Solution*

Thin accretion disks suffer from thermal and viscous instabilities under certain conditions (e.g., Pringle 1981, Frank et al. 1992). What are the stability properties of ADAFs?

Narayan & Yi (1995b) and Abramowicz et al. (1995) have shown that ADAFs are stable to long wavelength perturbations (see Narayan 1997 for a qualitative discussion of the relevant physics), while Kato et al. (1996, 1997) and Wu & Li (1996) showed that a one temperature ADAF may be marginally unstable to small scale perturbations. Using a time–dependent analysis, Manmoto et al. (1996) confirmed that density perturbations on small scales in a one-temperature ADAF do grow as the gas flows in, but not sufficiently quickly to affect the global validity of the solutions. They suggest that such perturbations may account for the variable hard X–ray emission which is observed in AGN and stellar mass black hole candidates. Recently, Wu (1997) has considered the stability of two temperature ADAFs to small scale fluctuations, and has shown that these flows are both viscously and thermally stable under most reasonable conditions.

3.3. *ADAF Plus Thin Disk Geometry: The Transition Radius*

Section 4 describes several applications of the ADAF model to X-ray binaries and AGN. Many of these applications utilize the following geometry, proposed by Narayan, McClintock, & Yi (1996). In this model, the accretion flow consists of two zones separated at a transition radius, r_{tr}. For $r < r_{tr}$, there is a two-temperature ADAF, whose properties are described in the previous two subsections. For $r > r_{tr}$, the accretion occurs partially as a thin accretion disk, and partially as a hot corona; the corona is modeled as an ADAF (Narayan, Barret, & McClintock 1997; Esin, McClintock, & Narayan 1997). The geometry is very similar to that proposed by SLE (see also Wandel & Liang 1991); the main difference is that the hot phase is taken to be a two-temperature ADAF, rather than the SLE solution.
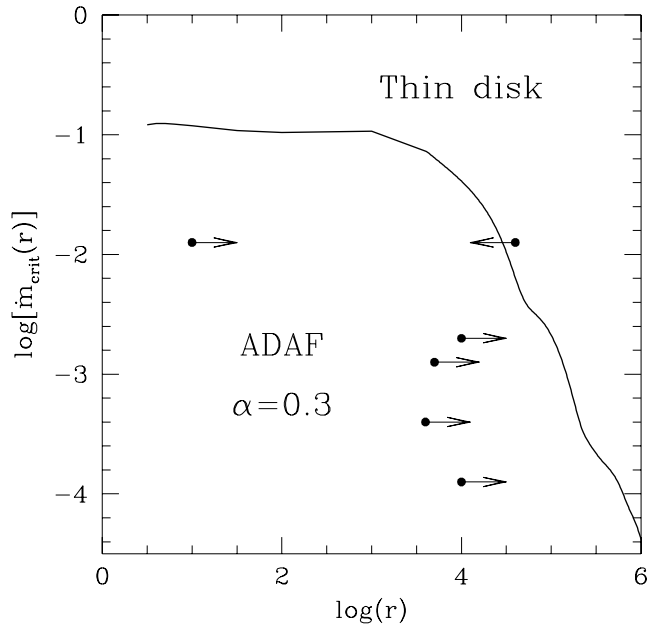
FIGURE 8. The solid line shows the estimated variation of $\dot{m}_{\mathrm{crit}}(r)$ with r. The horizontal segment up to $r = 10^3$ is from Esin et al. (1997) and the curve beyond that is based on a detailed model of optically thin cooling in a one-temperature gas (Menou et al. 1998). According to the "strong ADAF proposal" of Narayan & Yi (1995b), the curve also shows the variation of r_{tr} with $\dot{m}$. Regions above and to the right of the curve correspond to the thin disk solution, while regions below and to the left correspond to the ADAF. The dots and arrows show observationally derived limits on r_{tr}. The lower limits on r_{tr} are derived from fitting the spectra of various systems (from above: NGC 4258, V404 Cyg, GRO J1655-40, A0620–00, and Sgr A*), and also requiring the thin disk to be thermally stable in the thermal limit cycle model. The upper limit on r_{tr} in NGC4258 corresponds to the lowest radius at which maser emission has been detected. The calculated curve is consistent with the various constraints shown, but it is clear that fairly large changes are allowed, especially for $\dot{m} > 10^{-2.5}$.

Several proposals have been made to explain why the inflowing gas might switch from a thin disk to an ADAF at the transition radius. Meyer & Meyer–Hofmeister (1994) proposed, for cataclysmic variables, a mechanism in which the disk is heated by electron conduction from a hot corona; this evaporates the disk, leading to a quasi-spherical hot accretion flow. Honma (1996) suggested that turbulent diffusive heat transport from the inner regions of the ADAF produces a stable hot accretion flow out to large radii, which then joins to a cool thin disk. Narayan & Yi (1995b) suggested that small thermal instabilities in the optically-thin upper layers of a thin disk might cause the disk to switch to an ADAF. Other ideas are discussed by Ichimaru (1977) and Igumenshchev, Abramowicz, & Novikov (1997). It is not clear which, if any, of these mechanisms is most important.

It is generally believed that the transition radius r_{tr} is determined principally by $\dot{m}$, but the exact form of $r_{tr}(\dot{m})$ is not known. Narayan & Yi (1995b) suggested that, whenever the accreting gas has a choice between a thin disk and an ADAF, the ADAF

configuration is chosen. According to this (rather extreme) principle (the "strong ADAF principle"), $r_{tr}(\dot{m})$ is the maximum r out to which an ADAF is allowed for the given $\dot{m}$; equivalently, it is that r at which $\dot{m}_{\mathrm{crit}}(r) = \dot{m}$ (see Fig. 8). This prescription suggests that at low $\dot{m} \ll \dot{m}_{\mathrm{crit}} \sim \alpha^2$, r_{tr} will be very large even though a thin disk is perfectly viable at all radii. The evidence to date from quiescent X-ray binaries and galactic nuclei is consistent with this prediction (§4 and Fig. 8).

Even if the "strong ADAF proposal" of Narayan & Yi (1995b) is correct, it does not allow a reliable determination of $r_{tr}(\dot{m})$ because the precise form of $\dot{m}_{\mathrm{crit}}(r)$ is not known. The plot shown in Fig. (8) is based on fairly detailed computations by Esin et al. (1997) and Menou et al. (1998), but it still makes use of simplifying assumptions that may significantly influence the results.

4. Applications

ADAF models have been applied to a number of accreting black hole systems. They give a satisfying description of the spectral characteristics of several quiescent black hole binaries (Narayan et al. 1996, 1997b; Hameury et al. 1997) and low luminosity galactic nuclei (Narayan et al. 1995, 1998; Manmoto et al. 1997; Lasota et al. 1996; Reynolds et al. 1996; DiMatteo & Fabian 1997a) which are known to experience low efficiency accretion. ADAF models have also been applied successfully to more luminous systems which have higher radiative efficiencies (Esin et al. 1997, 1998).

The basic ADAF model has one adjustable parameter, $\dot{m}$; in principle, the transition radius r_{tr} is a second parameter, but most often the results are very insensitive to the choice of r_{tr}. In the future, the Kerr rotation parameter of the black hole will be an additional parameter of the models, but current models assume a Schwarzschild black hole. The mass of the black hole and inclination of the equatorial plane to the line of sight are estimated from observations, while the parameters describing the microphysics of the accretion flow are set to their canonical values (§3.1): $\alpha = 0.25$ or 0.30, $\beta = 0.5$, $\delta = 0.001$. (Any value of δ between 0 and 0.01 gives virtually identical results; see §3.2.3).

The X-ray flux is very sensitive to the density of the plasma and therefore to the accretion rate. For this reason, $\dot{m}$ is usually adjusted to fit the observed X-ray flux. The models described below are generally in good agreement with the remaining data that are not used in the fit: namely, the X-ray spectral slope, the optical/UV data, and, where available, the radio and infrared observations. In contrast, the thin disk model fits the observations very poorly.

The models presented here are the most up to date available, often more advanced than those in the literature; in particular, they include the compressive heating of electrons in the electron energy equation (see §3.2.3) and the full relativistic dynamics for accretion onto a Schwarzschild black hole (the photon transport includes gravitational redshift, but is otherwise Newtonian).

4.1. *Applications to X–Ray Binaries*

4.1.1. *Quiescent Black Hole Transients*

ADAF models have been used to explain the spectra of a number of quiescent black hole soft X–ray transients (SXTs), namely, A0620–00, V404 Cyg, and GRO J1655-40 (Narayan et al. 1996; Narayan et al. 1997b; Hameury et al. 1997). SXTs are mass transfer binaries in which the accreting star is often a black hole candidate (though sometimes a neutron star), and the companion star is usually a low–mass main sequence star (van Paradijs & McClintock 1995). Episodically, these systems enter a high luminosity, "outburst," phase, but for most of the time they remain in a very low luminosity,
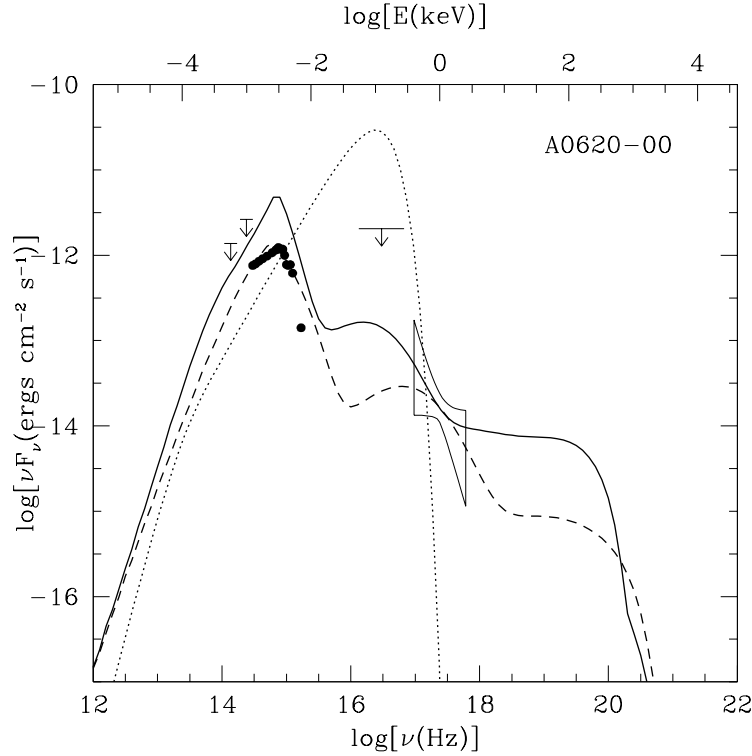
FIGURE 9. Spectrum of an ADAF model of A0620-00 (solid line) at an accretion rate of $\dot{m} = 4 \times 10^{-4}$, compared with the observational data. The dashed line is an ADAF model with $\beta = 0.8$, instead of the standard value of $\beta = 0.5$. The dotted line shows the spectrum of a thin accretion disk with an accretion rate $\dot{m} = 1 \times 10^{-5}$, adjusted to fit the optical flux. (Based on Narayan et al. 1997b)

"quiescent," phase. One problem with modeling quiescent SXTs is that a thin accretion disk cannot account for both the observed optical/UV and X–ray flux self–consistently. For example, in the case of A0620–00, a standard thin disk requires an accretion rate of $\dot{M} \sim 10^{-10} M_\odot \mathrm{yr}^{-1}$ to explain the optical/UV flux, while the X–ray flux requires an accretion rate of $\dot{M} \sim 10^{-15} M_\odot \mathrm{yr}^{-1}$ (McClintock et al. 1995). Another problem is that the optical spectrum resembles a blackbody with a temperature of $\sim 10^4$K, but a thin disk cannot exist at such a temperature since it would be thermally unstable (Wheeler 1996; Lasota et al. 1996a).

Narayan, McClintock, and Yi (1996) and Narayan et al. (1997b) resolved these problems using an ADAF + thin disk model with $r_{\mathrm{tr}} \sim 10^3 - 10^4$. The resulting spectra for A0620–00 and V404 Cyg are shown by solid lines in Figures 9 and 10. The ADAF models of the two sources reproduce the observed X-ray spectral slopes well; they also reproduce the optical/UV fluxes and spectral shapes reasonably well (note especially the good agreement in the position of the optical peak for A0620–00), though the optical flux is generally somewhat too luminous. Hameury et al. (1997) showed that observations of another SXT, GRO J1655-40, are also consistent with the presence of an ADAF in quiescence. The dotted lines in Figures (9) and (10) are steady state thin disk models adjusted to fit the optical flux; these models are clearly ruled out by the data.

The optical emission in the ADAF models of SXTs is due to synchrotron emission from the ADAF. The thin disk itself is very cool and is in a stable "low state." There is
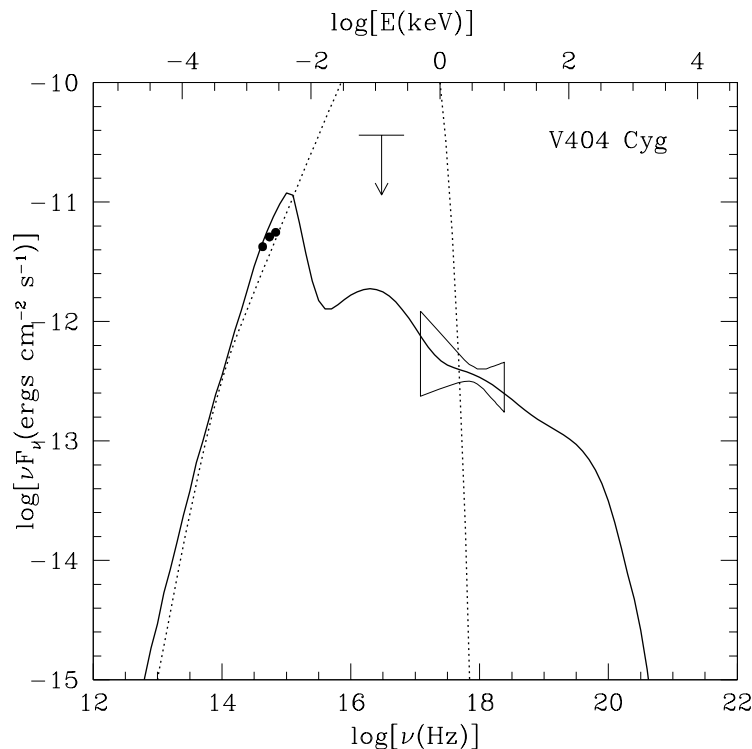
FIGURE 10. Spectrum of an ADAF model of V404 Cyg (solid line) at an accretion rate of $\dot{m} = 2 \times 10^{-3}$, compared with the observational data. The dotted line shows the spectrum of a thin accretion disk with $\dot{m} = 1.8 \times 10^{-3}$ (adjusted to fit the optical flux).

thus no difficulty with the thermal instability which a pure thin disk model would face in modeling the optical spectrum (Wheeler 1996; Lasota et al. 1996a). The ADAF model does overproduce the optical flux, but this can be fixed by changing the value of β from 0.5 to 0.8 (see the dashed line in figure 9).

4.1.2. *Clues From Outburst Timescales*

The above spectral models of quiescent SXTs require an inner ADAF which connects to an outer thin disk at a large transition radius. Lasota et al. (1996a) showed that a large transition radius can also be inferred from the outburst timescales of SXTs. In addition, optical and X–ray observations of the black hole SXT GRO J1655–40 showed an outburst in April of 1996. The optical outburst preceded the X-ray outburst by roughly 6 days (Orosz et al. 1997), which can be understood using an ADAF + thin disk model (but not using a pure thin disk extending down to the last stable orbit). See Lasota (this volume) for a detailed discussion of the implications of SXT outbursts for ADAF models.

4.1.3. *Spectral Models of Luminous X–Ray Binaries*

Narayan (1996a) proposed that the many different spectral states observed in black hole X-ray binaries can be understood as a sequence of thin disk + ADAF models with varying $\dot{m}$ and r_{tr}. These ideas have been worked out in more detail by Esin et al. (1997; 1998). A schematic diagram of their model is shown in Figure (11).

(*a*) Quiescent state: This lowest luminosity state has $\dot{m} \lesssim 10^{-2}$ and is discussed above (§4.1.1). Due to the low accretion rate, Comptonization is weak, and the X-ray flux is
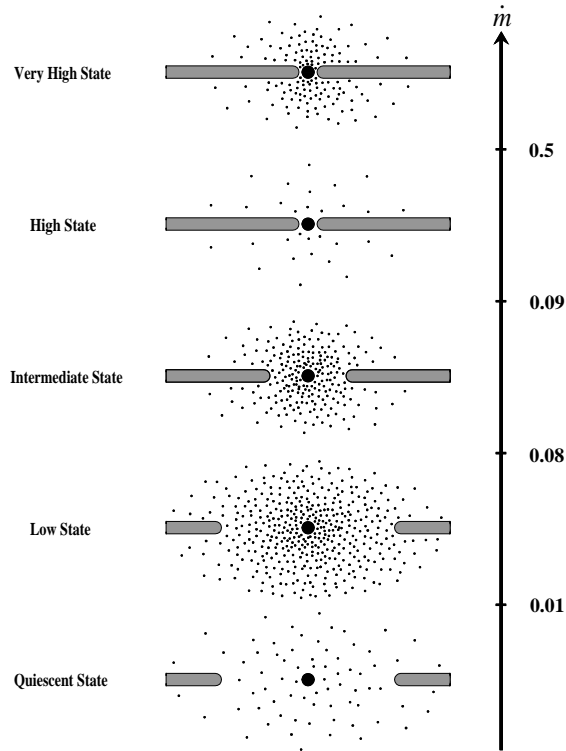
FIGURE 11. The configuration of the accretion flow in different spectral states shown schematically as a function of the total mass accretion rate $\dot{m}$ (from Esin et al. 1997). The ADAF is indicated by dots and the thin disk by the horizontal bars. The lowest horizontal panel shows the quiescent state which corresponds to a low mass accretion rate (and therefore, a low ADAF density) and a large transition radius. The next panel shows the low state, where the mass accretion rate is larger than in the quiescent state, but still below the critical value $\dot{m}_{\mathrm{crit}}$. In the intermediate state (the middle panel), $\dot{m} \sim \dot{m}_{\mathrm{crit}}$ and the transition radius is smaller than in the quiescent/low state. In the high state, the thin disk extends down to the last stable orbit and the ADAF is confined to a low-density corona above the thin disk. Finally, in the very high state, it has been suggested that the corona may have a substantially larger $\dot{m}$ than in the high state, but this is very uncertain.

much lower than the optical flux. The radiative efficiency is very low and the systems are extremely dim (cf. Figs. 6 and 7).

(b) Low state: For $\dot{m}$ above 10^{-2} and up to $\sim 10^{-1}$, the geometry of the accretion flow is similar to that of the quiescent state, but the luminosity and radiative efficiency are larger (and increase rapidly with $\dot{m}$). A low state spectrum of GRO J0442+32 is shown in figure (12). Comptonization becomes increasingly important, giving rise to a very hard spectrum which peaks around 100 keV.

(c) Intermediate state: At still higher accretion rates, $\dot{m}$ approaches $\dot{m}_{\mathrm{crit}} \sim 0.1$, the ADAF progressively shrinks in size, the transition radius decreases, and the X-ray spectrum changes continuously from hard to soft. This occurs at roughly constant bolometric luminosity. In this state, the thin disk becomes radiatively comparable to, or even brighter than, the ADAF.

(d) High state: At still higher accretion rates, $\dot{m} > \dot{m}_{\mathrm{crit}}$, the ADAF cannot exist as an independent entity at any radius, and the thin disk comes all the way down to the last stable orbit; there is, however, a weak corona above the thin disk which is modeled
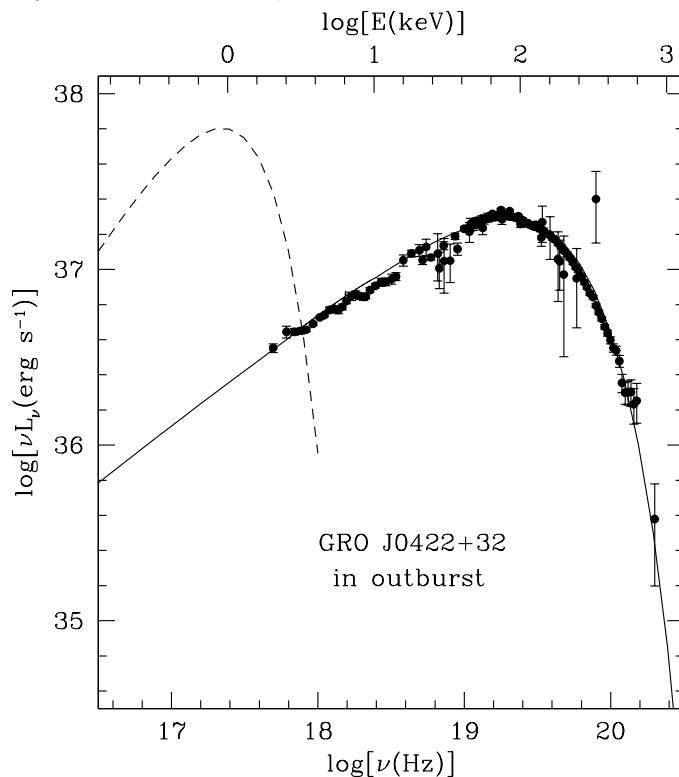
FIGURE 12. An ADAF model of J0442+32 (solid line) in the low state, compared with the observational data (dots and errorbars). The dashed line shows a thin disk model at the same accretion rate, $\dot{m} = 0.1$.

as an ADAF (with a coronal $\dot{m} \lesssim \dot{m}_{\rm crit}$). A characteristic high state spectrum resembles a standard thin disk spectrum, with a power law tail due to the corona.

This model accounts convincingly for the characteristic spectral state variations, from quiescence to the high state, seen in black hole X-ray binaries.

Esin et al. (1997; 1998) applied their model to the 1991 outburst of the SXT Nova Muscae and to the high-low/low-high state transition of Cyg X-1. Nova Muscae went into outburst during the fall of 1991, and was extensively studied in the optical and X–ray bands (Ebisawa et al. 1994; see also Brandt et al. 1992; Lund 1993; Goldwurm et al. 1992; Gilfanov et al. 1993). Its luminosity evolution is summarized in figure (13). The model light curves agree quite well with the data.

Figure (14) shows the broadband simultaneous RXTE (1.3-12 keV) and BATSE (20-600 keV) spectra of Cyg X-1 observed during the 1996 low-high (upper panel) and high-low (middle panel) state transitions. The bottom panel shows a sequence of ADAF + thin disk models, which are in good agreement with the observations. In particular, the model reproduces the range of photon indices seen in the data, the anti-correlation between the soft and hard X-ray flux, the "pivoting" around 10 keV, and the nearly constant bolometric luminosity throughout the transition.

One important result, highlighted by Narayan (1996), and confirmed by the more detailed calculations of Esin et al. (1997), is that the application of ADAFs to luminous black hole X-ray binaries requires a fairly large value of $\alpha \sim 0.25$. (The preliminary work of Narayan 1996 actually suggested $\alpha \sim 1$, but this was revised in Esin et al. 1997.) If
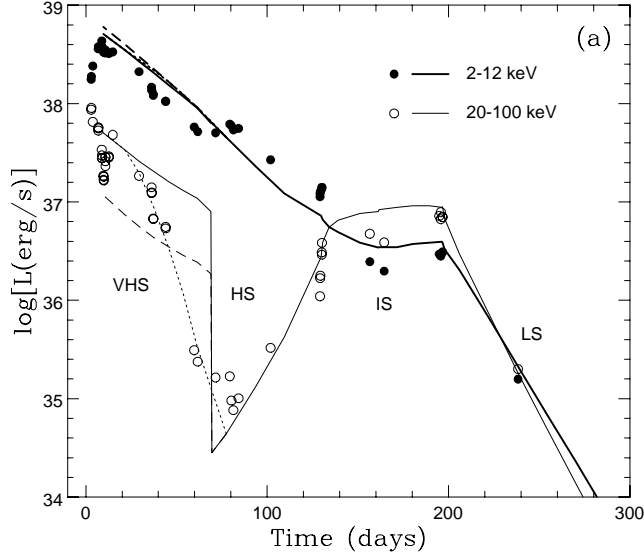
FIGURE 13. Soft and hard X-ray light curves of Nova Muscae 1991. Filled and open circles are data from Ebisawa et al. (1994) corresponding to the 2–12 keV and 20–100 keV bands, respectively. The heavy and thin lines are the model predictions (from Esin et al. 1997). The symbols VHS, HS, IS, LS correspond to the very high state, high state, intermediate state and low state, respectively. In the very high state, the solid, dotted, and dashed lines correspond to different prescriptions for viscous dissipation in the corona (see Esin et al. 1997 for details).

α is much smaller, then the ADAF solution cuts off at a very low mass accretion rate (recall that $\dot{m}_{\rm crit} \sim \alpha^2$), and the observed luminosities of low state systems cannot be explained. As discussed in §3.1, α will likely be large if the accreting gas has magnetic fields of equipartition strength.

Some black hole X-ray binaries, such as Nova Muscae 1991, exhibit an even higher luminosity state, called the very high state, which is significantly harder than the high state. This does not fit readily into the thin disk + ADAF paradigm. Esin et al. (1997) showed that if there is enhanced viscous dissipation of energy in the corona, as suggested by Haardt & Maraschi (1991, 1993) for modeling coronae in AGN, some properties of the very high state can be understood. Esin et al.'s model of the very high state is, however, quite speculative, and does not fit the observations particularly well.

4.2. *Applications to Galactic Nuclei*

4.2.1. *Sgr A**

Dynamical measurements of stellar velocities within the central 0.1 pc of the Galactic Center indicate a dark mass with $M \sim (2.5 \pm 0.4) \times 10^6 M_\odot$ (Haller et al. 1996; Eckart & Genzel 1997). This is believed to be the mass of the supermassive black hole in Sgr A*. Observations of stellar winds indicate that the expected accretion rate is $6 \times 10^{-6} M_\odot$ yr$^{-1} \leq \dot{M} \leq 2 \times 10^{-4} M_\odot$ yr^{-1} (Genzel et al. 1994; Melia 1992), which corresponds to
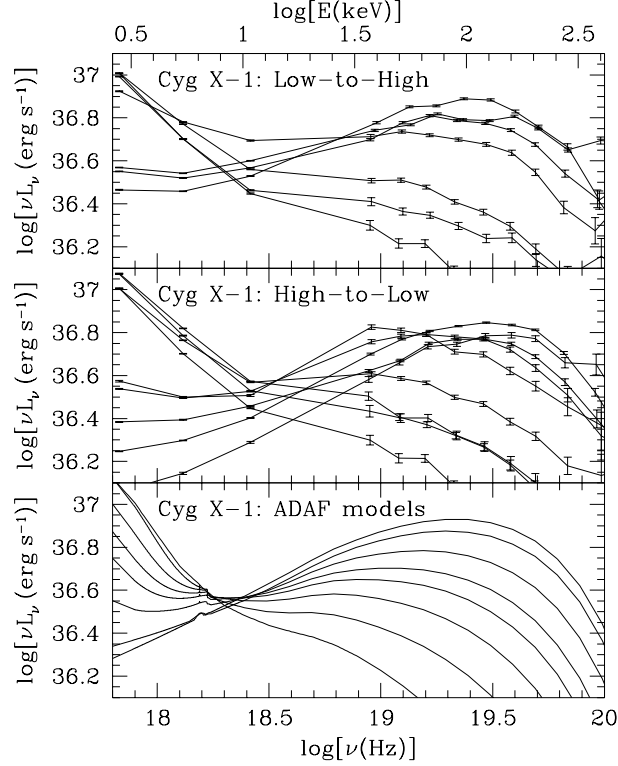
FIGURE 14. The RXTE (1.3-12 keV) and BATSE (20-600 keV) spectra of Cyg X-1 during the 1996 low-high (upper panel) and high-low (middle panel) state transitions. The bottom panel shows a sequence of ADAF + thin disk models which are in good agreement with the observations.

$10^{-4} \le \dot{m} \le 3 \times 10^{-3}$. Using a nominal radiative efficiency of 10% these accretion rates imply an accretion luminosity ($\sim 0.1\dot{M}c^2$) between $\sim 10^{40}$erg s^{-1} and $\sim 10^{42}$erg s^{-1}. Observations in the radio to γ–rays, however, seem to indicate a bolometric luminosity of less than 10^{37}erg s^{-1}. This extremely low luminosity has been used to argue against a supermassive black hole in Sgr A* (Mastichiadis & Ozernoy 1994; Goldwurm et al. 1994).

A standard thin disk with the above accretion rate gives rise to a black body spectrum which peaks in the near infrared (Frank et al. 1992). Menten et al. (1997), however, have obtained a strong upper limit on the infrared emission from the Galactic center, and find it to be below $\sim 10^{34}$erg s^{-1}. This effectively rules out any thin disk model of the Galactic Center.

All of the apparently contradictory observations of Sgr A* appear to be naturally accounted for by an optically thin, two temperature, ADAF model. Rees (1982) first suggested that Sgr A* may be advecting a significant amount of energy and Narayan et al. (1995) provided the first spectral model; more detailed recent models (Manmoto et al. 1997; Narayan et al. 1998) confirm that an ADAF model can explain the observations quite well. The solid line in Figure (15a) shows the best fit Narayan et al. (1998) model, while the dotted lines correspond to thin disk models, which are easily ruled out by the data. The mass of the central black hole is fixed at its dynamically measured value of $2.5 \times 10^6 M_\odot$ and the accretion rate is varied to fit the X–ray flux. The resulting accretion
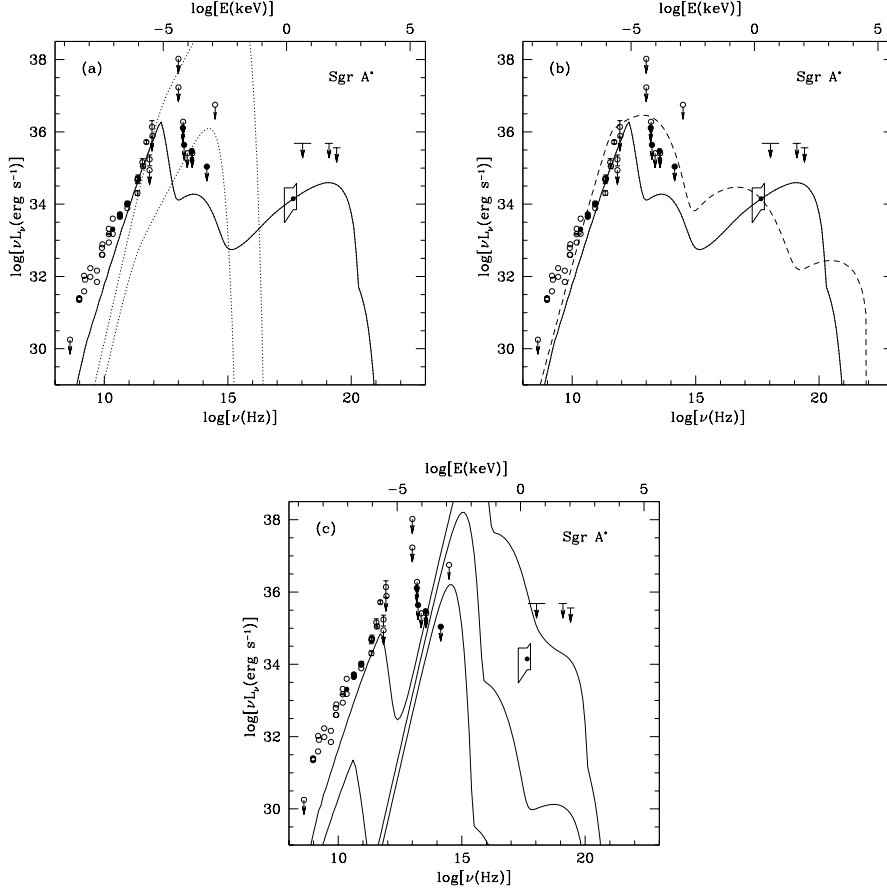
FIGURE 15. (a) Spectrum of a two temperature ADAF model of Sgr A* (solid line). The mass accretion rate inferred from this model is $\dot{m} = 1.3 \times 10^{-4}$, in agreement with an independent observational determination. Dotted lines show the spectra of thin accretion disks, at the same accretion rate (upper) and at $\dot{m} = 10^{-8}$ (lower). (b) The dashed line is a one temperature ADAF model of Sgr A* at $\dot{m} = 3 \times 10^{-7}$ (adjusted to fit the x-ray flux). The solid line is the standard two temperature model. (c) Spectra of ADAF models of Sgr A* where the central star is taken to have a hard surface at $r = 3$ and the advected energy is assumed to be reradiated from the surface as a blackbody. The three spectra correspond to $\dot{m} = 10^{-4}, 10^{-6}$, and 10^{-8} (from top to bottom). All three models violate the infrared limits.

rate is $\dot{m} \sim 1.3 \times 10^{-4}$, which is consistent with the mass accretion rate estimates from the observations of stellar winds.

The resulting model naturally reproduces the observed spectrum in other wavebands. Synchrotron radiation from the ADAF produces the radio spectrum which cuts off sharply in the sub–mm; the inverse Compton spectrum is consistent with the stringent upper limit on the NIR flux given by Menten et al. (1997); finally, bremsstrahlung radiation is responsible for the X–ray flux which extends up to a few hundred keV. There is, however, a problem at low radio frequencies, $\lesssim 10^{10}$ Hz, where the model is well below the observed flux. In addition, the γ–ray spectrum from the ADAF is lower than the observed flux by nearly an order of magnitude (not shown in Figure 15; see Figure 1 of Narayan et al. (1998)). The latter is not considered to be a serious problem since it is unclear whether the observed γ–rays are in fact from a point or a diffuse source at the Galactic Center.
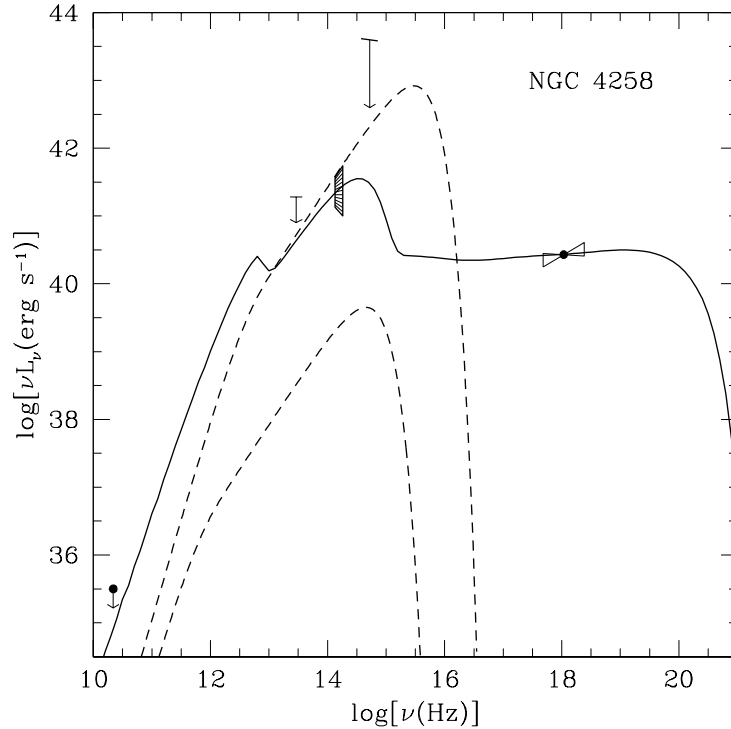
FIGURE 16. Spectrum of an ADAF model of NGC 4258 (solid line), at an accretion rate of $\dot{m} = 9 \times 10^{-3}$ with a transition radius of $r_{tr} = 30$. Dotted lines show the spectra of thin accretion disks at accretion rates of $\dot{m} = 4 \times 10^{-3}$ (upper, adjusted to fit the infrared points) and $\dot{m} = 10^{-5}$ (lower).

Sgr A* is one of the few observed systems for which the luminosity is low enough that a one temperature ADAF model can be constructed (recall from §3.2.2 that $\dot{m}_{\rm crit} \sim 10^{-6}$ for a one temperature ADAF so that a source must have a luminosity $\lesssim 10^{-6}L_{\rm edd}$ for a one temperature ADAF model to be possible). This model (dashed line in Figure 15b) is, however, ruled out by the data.

An important feature of the two temperature ADAF model of Sgr A* is that the observed low luminosity is explained as a natural consequence of the advection of energy in the flow, rather than as a very low accretion rate (the radiative efficiency is very low, $\sim 5 \times 10^{-6}$). The model will not work if the central object has a hard surface and reradiates the advected energy, as demonstrated in Figure (15c). Therefore, the success of the ADAF model implies that Sgr A* is a black hole with an event horizon (§4.3).

4.2.2. *NGC 4258*

The mass of the central black hole in the AGN NGC 4258 has been measured to be $3.6 \times 10^7 M_\odot$ (Miyoshi et al. 1997). Observations of water masers indicate the presence of a thin disk, at least at large radii. Highlighting the fact that the observed optical/UV and X-ray luminosities are significantly sub-Eddington ($\sim 10^{-4}$ and $\sim 10^{-5}$, respectively), Lasota et al. (1996) proposed that the accretion in NGC 4258 at small radii proceeds through an ADAF. In Lasota et al.'s original model, the transition radius was a free parameter, but since then new infrared observations have been made (Chary & Becklin 1997) that constrain the transition radius to be $r_{tr} \sim 30$. The outer thin disk then accounts for the

newly observed infrared emission, and the refined model (see Fig. 16, based on Gammie, Narayan & Blandford 1998) is also in agreement with a revised (smaller) upper limit on the radio flux from NGC 4258 (Herrnstein et al. 1998). Maoz & McKee (1997) and Kumar (1997) find, via quite independent arguments, an accretion rate for NGC 4258 in agreement with the ADAF model ($\dot{m} \sim 0.01$). Neufeld & Maloney (1995) estimate a much lower $\dot{m} < 10^{-5}$ in the outer maser disk via a model of the maser emission. The accretion rate close to the black hole cannot be this low; not even an efficiently radiating thin disk can produce the observed infrared and X-ray radiation with such an $\dot{m}$ (the lower dotted line in Fig. 16).

4.2.3. *Other Low Luminosity Galactic Nuclei*

ADAFs have also been used to model a number of other nearby low luminosity galactic nuclei, e.g., M87 (Reynolds et al. 1996) and M60 (Di Matteo & Fabian 1997a) in the Virgo cluster. These and similar elliptical galaxies are believed to have contained quasars with black hole masses $\sim 10^{8}-10^{9} M_{\odot}$ at high redshift (Soltan 1982; Fabian & Canizares 1988; Fabian & Rees 1995). In the case of M87 and several other galaxies there is independent evidence for such dark mass concentrations in their centers (Ford et al. 1997). The unusual dimness of these galactic nuclei is, however, a problem.

Fabian & Canizares (1988) considered six bright nearby ellipticals and, using X–ray gas profiles in the central arcsecond regions, estimated the accretion rates onto the central black holes. For a standard radiative efficiency of 0.1, their estimated accretion rates yielded luminosities which were substantially larger than the observed luminosities. Thus these galactic nuclei appeared to be very underluminous. Fabian & Canizares (1988) highlighted this problem, calling it the dead quasar problem. As suggested by Fabian & Rees (1995), and confirmed by the detailed calculations of Mahadevan (1997), the problem is naturally resolved if the galactic nuclei are presently accreting via an ADAF, rather than a thin disk. ADAFs are naturally underluminous and have low radiative efficiencies. Similarly, Lasota et al. (1996b) suggested that perhaps all LINERs (of which NGC 4258 is an example) have ADAFs.

4.2.4. *AGN Statistics*

Quasars first appear at a redshift $z \sim 5$ and their numbers increase with decreasing z; below a redshift ~ 2, however, the number of quasars decreases rapidly. Quasars are essentially non–existent at the present epoch, $z \sim 0$. In the standard AGN paradigm, all quasars are assumed to be powered by accretion onto supermassive black holes. Yi (1996) has suggested (following Fabian & Rees 1995) that quasars may switch from accretion via a thin disk to accretion via an ADAF at $1 \lesssim z \lesssim 2$; this provides a natural explanation for the decrease in quasar number counts at small z since ADAFs are significantly less luminous and thus much more difficult to detect. What accounts, however, for the change in the accretion mechanism at $z \sim 2$? Yi assumes that at large z, quasars accrete at $\dot{m} \sim 1$, and so the accretion must be via a thin disk. As the quasar evolves, however, two processes lead to decreasing $\dot{m}$: (1) A decrease in the fuel supply, and (2) an increase in the mass of the accreting black hole; since $\dot{m} \propto \dot{M}/M$, both of these cause $\dot{m}$ to decrease and lead to a critical redshift below which $\dot{m} \lesssim \dot{m}_{\rm crit}$; at this point ($z \sim 2$), the accretion flow switches to an ADAF.

4.2.5. *The X-Ray Background*

Di Matteo & Fabian (1997b; see also Yi & Boughn 1998) argue that ADAFs can be used to model the diffuse X–ray background. The spectrum of the diffuse XRB resembles thermal bremsstrahlung in the 3–60 keV range, and has a rollover at ~ 30
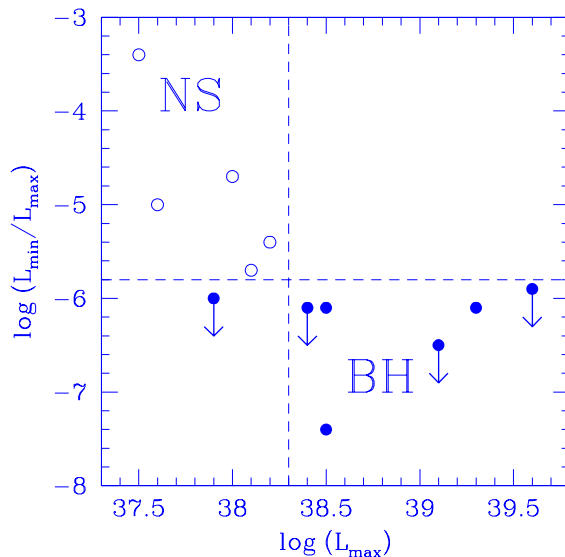
FIGURE 17. A comparison between black hole (BH, filled circles) and neutron star (NS, open circles) SXT luminosity variations (from Narayan et al. 1997c and Garcia et al. 1998). The ratio of the quiescent luminosity to the peak outburst luminosity is systematically smaller for BH systems than for NS systems. This indicates the presence of event horizons at the center of BH candidate systems.

keV. The X–ray background is thought to arise from many discrete sources. ADAFs are a natural candidate since (1) they intrinsically produce bremsstrahlung, (2) the electron temperature is in the right range, $\sim 10^9$K, to account for the observed cutoff, and (3) the electron temperature is very insensitive to the parameters of the model. Assuming a modest spectral evolution with redshift, Di Matteo & Fabian (1997b) were able to reproduce the X–ray background fairly well. Since moderately high accretion rates are required to account for the observed flux, however, Comptonization contributes to the hard X–ray spectrum of the ADAFs. Di Matteo & Fabian avoid this problem by invoking a high degree of clumpiness in the gas so that bremsstrahlung emission dominates over Compton scattering, but this is somewhat ad hoc.

4.3. *Evidence for the Black Hole Event Horizon*

A unique feature of the ADAF applications described above is that the models require the existence of an event horizon in the central object (Narayan et al. 1996; Narayan et al. 1997bc). Since the protons store most of the viscous energy as thermal energy as they fall onto the central object, the luminosity from the ADAF is much less than the viscously generated energy ($\sim 0.1 \dot{M} c^2$). If the central object had a hard surface, this thermal energy would be reprocessed and reradiated, resulting in a net luminosity from the object $\sim 0.1 \dot{M} c^2$; the spectrum would also differ significantly from that of a pure ADAF (since it would be dominated by the reprocessed radiation; see Figure 15 as an

example). If the central object is a black hole, however, the advected thermal energy is carried into the black hole through the event horizon, and is "lost" to the outside observer. The success of ADAF models of the various black hole candidates discussed in the previous sections *without* reprocessed radiation therefore indicates the presence of an event horizon in all of these objects.

Narayan et al. (1997c; see also Yi et al. 1996) highlighted the distinction between black holes and compact stars with surfaces in a different way by comparing the luminosities of black hole and neutron star soft X–ray transients in outburst and quiescence. In outburst, the accretion rates in both neutron star and black hole systems are high, $\dot{m} \sim 1 \gtrsim \dot{m}_{\rm crit}$, and the accretion occurs via a standard thin disk. The observed outburst luminosities, L_{max}, should therefore be proportional to $\dot{M} \propto m$. This is consistent with the observation that black hole SXTs in outburst have a larger L_{max} than neutron star SXTs, as expected because of their larger mass.

In quiescence, the accretion rates are low, $\dot{m} \ll \dot{m}_{\rm crit}$, and the accretion occurs via an ADAF. Since neutron stars have hard surfaces, however, the advected energy is ultimately reradiated, and the luminosity is still proportional to $\dot{m}$. For an ADAF around a black hole, on the other hand, the advected energy is not reradiated, but is deposited into the black hole. The quiescent luminosities, L_{min}, from black hole candidates should therefore be substantially less, roughly proportional to $\dot{m}^2$ (see Fig. 7). Black hole SXTs should thus experience more substantial luminosity changes from quiescence to outburst than neutron star SXTs. As figure (17) shows, this is exactly what is observed. This provides additional evidence for the existence of event horizons in black hole candidates.

5. Conclusion

The two-temperature ADAF model provides a consistent framework for understanding the dynamics and spectra of black hole accretion flows at low mass accretion rates, $\dot{m} \lesssim 0.1$. By modeling coronae as ADAFs, the model is also being extended successfully to systems with $\dot{m} \gtrsim 0.1$, though not yet to systems close to the Eddington limit ($\dot{m} \sim 1$).

The field is young and there are many open questions. Perhaps the most fundamental issue is whether the assumptions underlying the two-temperature ADAF model are valid (§3.1). Another major question, where much work needs to be done, is the physics underlying the transition radius (§3.3). If this is understood, and the dynamics and thermal structure of the corona can be modeled well, it will be possible to calculate $r_{tr}(\dot{m})$ reliably; this will be an enormous improvement over the present work. Improvements are necessary in the modeling techniques as well. Fully relativistic computations of the coupled dynamics and radiative transfer will be welcome. One needs to include time-dependence in the models in order to understand the complex variations of spectra with time, especially in X-ray binaries such as the SXTs. Ultimately, we expect that time-dependent two-dimensional simulations will elevate the ADAF model to a fully quantitative tool, though this is probably many years away.

Two wider issues should be highlighted. First, the high-$\dot{m}$, optically thick, ADAF (corresponding to radiation trapping) has not been explored at the level of detail of the low $\dot{m}$, two-temperature, ADAF. More quantitative models, especially with respect to their spectral properties, would be worthwhile. It is possible that some of the presently most puzzling sources (e.g. SS433) correspond to this branch of ADAFs. The other issue has to do with jets and outflows. There are tantalizing hints that ADAFs may be particularly efficient at producing outflows (Narayan & Yi 1994, 1995a), but the connection has not been developed in any detail.

REFERENCES

Abramowicz, M., Chen, X., Kato, S., Lasota, J. P, & Regev, O., 1995, *The Astrophysical Journal Letters*, **438**, L37.

Abramowicz, M., Czerny, B., Lasota, J. P., & Szuszkiewicz, E., 1988, *The Astrophysical Journal*, **332**, 646.

Abramowicz, M., Jaroszyński, M., & Sikora, M., 1978, *Astronomy & Astrophysics*, **63**, 221.

Abramowicz, M., Chen, X., Granath, M., & Lasota, J.–P., 1996, *The Astrophysical Journal*, **471**, 762.

Achterberg, A. 1981, *Astronomy & Astrophysics*, **97**, 259.

Balbus, S. A., & Hawley, J. F. 1991, *The Astrophysical Journal*, **376**, 214.

Begelman, M. C., 1978, *Monthly Notices of the Royal Astronomical Society*, **243**, 610.

Begelman, M. C., & Chiueh, T., 1988, *The Astrophysical Journal*, **332**, 872.

Begelman, M. C., & Meier, D. L., 1982, *The Astrophysical Journal*, **253**, 873.

Bisnovatyi-Kogan, G.S. & Lovelace, R. V. E. 1997, *The Astrophysical Journal Letters*, **486**, L43.

Björnsson, G., Abramowicz, M. , Chen, X., Lasota, J.–P., 1996, *The Astrophysical Journal*, **467**, 99.

Björnsson, G. & Svensson, R., 1991, *The Astrophysical Journal Letters*, **379**, L69.

Blackman, E. 1998, *Physical Review Letter*, in press (astro-ph/9710137).

Bondi, H., 1952, *Monthly Notices of the Royal Astronomical Society*, **112**, 195.

Brandt, S., Castro–Tirado, A. J., Lund, N., Dremin, V., Lapshov, I., & Sunyaev, R. A., 1992, *Astronomy & Astrophysics*, **254**, L39.

Celotti, A., Fabian, A. C., & Rees, M. J. 1997, *Monthly Notices of the Royal Astronomical Society*, **293**, 239. (astro–ph/9707131).

Chakrabarti, S. K. 1990, *Monthly Notices of the Royal Astronomical Society*, **243**, 610.

Chakrabarti, S. K., & Titarchuk, L. G. 1995, *The Astrophysical Journal*, **455**, 623.

Chakrabarti, S. K. 1996, Physics Reports, **266**, 229.

Chary, R. & Becklin, E. E., 1997 *The Astrophysical Journal Letters*, **485**, L75.

Chen, X. 1995, *Monthly Notices of the Royal Astronomical Society*, **275**, 641.

Chen, X., Abramowicz, M. A., Lasota, J.-P., Narayan, R., & Yi, I. 1995, *The Astrophysical Journal Letters*, **443**, 61.

Chen, X., Abramowicz, M. A., & Lasota, J.-P., 1997, *The Astrophysical Journal*, **476**, L61.

Di Matteo, T., & Fabian, A. C., 1997a, *Monthly Notices of the Royal Astronomical Society*, **286**, 50.

Di Matteo, T., & Fabian, A. C., 1997b, *Monthly Notices of the Royal Astronomical Society*, **286**, 393.

Ebisawa, K., et al., 1994, *Publications of the Astronomical Society of Japan*, **46**, 375.

Eckart, A., & Genzel, R., 1997, *Monthly Notices of the Royal Astronomical Society*, **284**, 576.

Eggum, G. E., Coroniti, F. V., & Katz, J. I., 1988, *The Astrophysical Journal*, **330**, 142.

Esin, A. A., 1997, *The Astrophysical Journal*, **482**, 400.

Esin, A. A., McClintock, J. E., & Narayan, R., 1997, *The Astrophysical Journal*, **489**, 865.

Esin, A. A., Narayan, R., Cui, W., Grove, J. E., & Zhang, S-N. 1998, *The Astrophysical Journal*, in press.

Esin, A. A., Narayan, R., Ostriker, E., & Yi, I. 1996, *The Astrophysical Journal*, **465**, 312.

Fabian, A. C., & Canizares, C. R., 1988, *Nature*, **333**, 829.

Fabian, A. C., & Rees, M. J., 1995, *Monthly Notices of the Royal Astronomical Society*, **277**, L5.

Fishbone, L. G., & Moncrief, V., 1976, *The Astrophysical Journal*, **207**, 962.

Ford, H. C., Tsvetanov, Z. I., Ferrarese, L., and Jaffe, W. in proc. IAU Symp. 184, *The Central Region of the Galaxy and Galaxies*, ed. Y. Sofue (1997).

Frank, J., King, A., & Raine, D., 1992, in *Accretion Power in Astrophysics*. Cambridge Univ. Press.

Fujita, Y. et al. 1998, *The Astrophysical Journal Letters*, in press.

Gammie, C. F., Narayan, R. & Blandford, R. 1998, in preperation.

Gammie, C. F. & Popham, R. G., 1998, *The Astrophysical Journal*, in press (astro–ph/9705117).

Garcia et al. 1998, in *Proc. 13th NAW on CV's*, eds. S. Howell, E. Kuulkers, & C. Woodward.

Genzel, R., Hollenbach, D., & Townes, C. H., 1994, *Rep. Prog. Phys.,* **57**, 417.

Ghisellini, G. & Svensson, R. 1990, in *Physical Processes in Hot Cosmic Plasmas*, ed. W. Brinkmann, A.C. Fabian, & F. Giovannelli (NATO AI Ser. C, 305) (Dordrecht: Kluwer), p. 395.

Ghisellini, G. & Svensson, R. 1991, *Monthly Notices of the Royal Astronomical Society*, **252**, 313.

Gilfanov, M., et al., 1993, *Astronomy & Astrophysics Supplement*, **97**, 303.

Goldreich, P. & Sridhar, S. 1995, *The Astrophysical Journal*, **438**, 763.

Goldwurm, A., et al., 1994, *Nature*, **371**, 589.

Gruzinov, A., 1998, *The Astrophysical Journal*, in press (astro-ph/9710132).

Haardt, F., & Maraschi, L., 1991, *The Astrophysical Journal Letters*, **380**, L51.

Haardt, F., & Maraschi, L., 1993, *The Astrophysical Journal*, **413**, 507.

Haller, J., Rieke, M. J., Rieke, G. H., Tamblyn, P., Close, L., & Melia, F., 1996, *The Astrophysical Journal*, **468**, 955.

Hameury, J.–M., Lasota, J.–P., McClintock, J. E., & Narayan, R., 1997, *The Astrophysical Journal*, **489**, 234 (astro–ph/9703095).

Hawley, J. F., Gammie, C. F., & Balbus, S. A., 1996, *The Astrophysical Journal*, **464**, 690.

Herrnstein et al., 1998, in preparation.

Huang, M., & Wheeler, J. C, 1989, *The Astrophysical Journal*, **343**, 229.

Honma, F., 1996, *Publications of the Astronomical Society of Japan*, **48**, 77.

Ichimaru, S., 1977, *The Astrophysical Journal*, **214**, 840.

Igumenshchev, I. V., Abramowicz, M. A., & Novikov, I. D. 1998, *Monthly Notices of the Royal Astronomical Society*, in press (astro–ph/9709156).

Igumenshchev, I. V., Chen, X., & Abramowicz, M. A. 1996, *Monthly Notices of the Royal Astronomical Society*, **278**, 236.

Kato, S., Yamasaki, T., Abramowicz, M. A., & Chen, X., 1997, *Publications of the Astronomical Society of Japan*, **49**, 221.

Kato, S., Abramowicz, M. A., & Chen, X., 1996, *Publications of the Astronomical Society of Japan*, **48**, 67.

Katz, J., 1977, *The Astrophysical Journal*, **215**, 265.

Kumar, P. 1998, *The Astrophysical Journal*, in press.

Kusunose, M. & Mineshige, S., 1996, *The Astrophysical Journal*, **468**, 330.

Lasota, J.-P., Narayan, R., & Yi, I., 1996, *Astronomy & Astrophysics*, **314**, 813.

Lasota, J.-P., Abramowicz, M. A., Chen, X., Krolik, J., Narayan, R., & Yi, I., 1996, *The Astrophysical Journal*, **462**, 142.

Lund, N., 1993, *Astronomy & Astrophysics Supplement*, **97**, 289.

Luo, C. & Liang, E. P., 1994 *Monthly Notices of the Royal Astronomical Society*, **266**, 386L.

LYNDEN–BELL, D., & PRINGLE, J. E., 1974, *Monthly Notices of the Royal Astronomical Society*, **168**, 603.

MAHADEVAN, R., 1997, *The Astrophysical Journal*, **477**, 585.

MAHADEVAN, R., NARAYAN, R., & KROLIK, J., 1997, *The Astrophysical Journal*, **486**, 268.

MAHADEVAN, R., NARAYAN, R., & YI, I., 1996, *The Astrophysical Journal*, **465**, 327.

MAHADEVAN, R., & QUATAERT, E., 1997, *The Astrophysical Journal*, **490**, 605.

MANMOTO, T., TAKEUCHI, M., MINESHIGE, S., MATSUMOTO, R., & NEGORO, H., 1996, *The Astrophysical Journal*, **464**, L135.

MANMOTO, T., MINESHIGE, S., & KUSUNOSE, M. 1997, *The Astrophysical Journal Letters*, **489**, 791.

MAOZ, E. & MCKEE, C. F. 1998, *The Astrophysical Journal*, **494**, 218.

MASTICHIADIS, A. & OZERNOY, L. M., 1994, *The Astrophysical Journal*, **426**, 599.

MATSUMOTO, R., KATO, S., & FUKUE, J. 1985 in *Theoretical Aspects on Structure, Activity, and Evolution of Galaxies III*, eds. S. Aoki, M. Iye, &Y. Yoshii (Tokyo Astr. Obs: Tokyo), p. 102.

MCCLINTOCK ET AL. 1995, *The Astrophysical Journal*, **442**, 358.

MELIA, F. 1992, *The Astrophysical Journal Letters*, **387**, L25.

MENOU, K., NARAYAN, R., & LASOTA, J. P., 1998, in preparation.

MENTEN, K. M., REID, M. J., ECKART, A., & GENZEL, R., 1997, *The Astrophysical Journal Letters*, **475**, L111.

MEYER, F., & MEYER–HOFMEISTER, E., 1994, *Astronomy & Astrophysics*, **288**, 175.

MINESHIGE, S., & WHEELER, J. C., 1989, *The Astrophysical Journal*, **343**, 241.

MIYOSHI, M., MORAN, J., HERRNSTEIN, J., GREENHILL, L., NAKAI, N., DIAMOND, P., & INOUE, M., 1995, *Nature*, **373**, 127.

NAKAMURA, K. E., KUSUNOSE, M., MATSUMOTO, R., & KATO, S. 1997, *Publications of the Astronomical Society of Japan*, **49**, 503.

NAKAMURA, K. E., MATSUMOTO, R., KUSUNOSE, M., & KATO, S. 1996, *Publications of the Astronomical Society of Japan*, **48**, 761.

NARAYAN, R., 1996a, *The Astrophysical Journal*, **462**, 136.

NARAYAN, R., 1996b, in *Physics of Accretion Disks*, (eds. S. Kato, S. Inagaki, S. Mineshige, J. Fukue). p15. Gordan & Breach.

NARAYAN, R., & YI, I., 1994, *The Astrophysical Journal Letters*, **428**, L13.

NARAYAN, R., & YI, I., 1995a, *The Astrophysical Journal*, **444**, 231.

NARAYAN, R., & YI, I., 1995b, *The Astrophysical Journal*, **452**, 710.

NARAYAN, R., YI, I., & MAHADEVAN, R., 1995, *Nature*, **374**, 623.

NARAYAN, R., MCCLINTOCK, J. E., & YI, I. 1996, *The Astrophysical Journal*, **457**, 821.

NARAYAN, R. 1997, in *Accretion Phenomena & Related Outflows, Proc. IAU Colloq. 163 A.S.P. Conf. Series* (eds. D. T. Wickramasinghe, L. Ferrario, G. V. Bicknell).

NARAYAN, R., KATO, S., & HONMA, F. 1997a, *The Astrophysical Journal*, **476**, 49.

NARAYAN, R., BARRET, D., & MCCLINTOCK, J. 1997b, *The Astrophysical Journal*, **482**, 448.

NARAYAN, R., GARCIA, M. R., & MCCLINTOCK, J. 1997c, *The Astrophysical Journal Letters*, **478**, L79.

NARAYAN, R., MAHADEVAN, R., GRINDLAY, J. E., POPHAM, R. G., & GAMMIE, C. 1998, *The Astrophysical Journal*, **492** (astro–ph/9706112).

NEUFELD, D. A. & MALONEY, P. R. 1995, *The Astrophysical Journal Letters*, **447**, L17.

NOVIKOV, I. D., & THORNE, K. S. 1973, in *Blackholes* (ed. C. DeWitt & B. DeWitt), 343. Gordon & Breach.

OROSZ, J. A., REMILLARD, R. A., BAILYN, C. D., & MCCLINTOCK, J. E. 1997, *The Astrophysical Journal*, **478**, 83.

PACZYŃSKI, B., & WIITA, P. J. 1980, *Astronomy & Astrophysics*, **88**, 23.

PEITZ, J., & APPL, S. 1997, *Monthly Notices of the Royal Astronomical Society*, **286**, 681 (astro–ph/9612205).

PHINNEY, E. S. 1981 in *Plasma Astrophysics*, ed. T. Guyenne (ESA SP-161), p. 337.

PIRAN, T. 1978, *The Astrophysical Journal*, **221**, 652.

POPHAM, R. G., & GAMMIE, C. F., 1998, *The Astrophysical Journal*, in press.

PRINGLE, J. E. 1981, *Annual Reviews of Astronomy & Astrophysics*, **19**, 137.

QUATAERT, E., 1998, *The Astrophysical Journal*, in press (astro-ph/9710127).

QUATAERT, E. & GRUZINOV, A. 1998, Apj submitted (astro-ph/9803112)

REES, M. J. 1982, in *The Galactic Center* (ed. G. R. Riegler & R. D. Blandford). AIP, p166. New York.

REES, M. J., BEGELMAN, M. C., BLANDFORD, R. D., & PHINNEY, E. S. 1982, *Nature*, **295**, 17.

REYNOLDS, C. S., DI MATTEO, T., FABIAN, A. C., HWANG, U., & CANIZARES, C. R. 1996, *Monthly Notices of the Royal Astronomical Society*, 1996, **283**, L111.

SHAKURA, N. I., & SUNYAEV, R. A. 1973, *Astronomy & Astrophysics*, **24**, 337.

SHAKURA, N. I., & SUNYAEV, R. A. 1976, *Monthly Notices of the Royal Astronomical Society*, **175**, 613.

SHAPIRO, S. L., LIGHTMAN, A. P., & EARDLEY, D. M. 1976, *The Astrophysical Journal*, **204**, 187 (SLE).

SOLTAN, A. 1982, *Monthly Notices of the Royal Astronomical Society*, **200**, 115.

SPITZER, L. JR. 1962, *Physics of Fully Ionized Gases*, 2nd Ed. John Wiley & Sons, Inc.

SPRUIT, H.C., MATSUDA, T., INOUE, M., & SAWADA, K. 1987, *Monthly Notices of the Royal Astronomical Society*, **229**, 517.

SZUSKIEWICZ, E., MALKAN, M. A., & ABRAMOWICZ, M. A. 1996, *The Astrophysical Journal*, **458**, 474.

VAN PARADIJS, J. & MCCLINTOCK, J. E., 1995, in *X-Ray Binaries*, ed. W. H. G. Lewin et al. (Cambridge: Cambridge Univ. Press), p. 58.

WANDEL, A. & LIANG, E. P., 1991, *The Astrophysical Journal Letters*, **376**, 746L.

WHEELER, C. J., 1996, in *Relativistic Astrophysics*, eds. B. Jones & D. Markovic (Cambridge: Cambridge University press)

WU, X. 1997, *Monthly Notices of the Royal Astronomical Society*, **292**, 113 (astro–ph/9707329).

WU, X., & LI, Q. 1996, *The Astrophysical Journal*, **469**, 776.

YI, I., & BOUGHN, S. P. 1998, *The Astrophysical Journal*, in press (astro–ph/9710147).

YI, I. 1996, *The Astrophysical Journal*, **473**, 645.

YI, I., NARAYAN, R., BARRET, D., & MCCLINTOCK, J. E. 1996, *Astronomy & Astrophysics Supplement*, **120**, 187.